NUMERICAL ANALYSIS ON THE GENERATION OF EQUILIBRIUM AEOLIAN SEDIMENTARY BED-FORMS FROM RANDOM SURFACES

A Thesis

by

CHANDAN TANKALA

Submitted to the Office of Graduate Studies of
Texas A&M University
in partial fulfillment of the requirements for the degree of

MASTER OF SCIENCE

August 2012

Major Subject: Geophysics

NUMERICAL ANALYSIS ON THE GENERATION OF EQUILIBRIUM AEOLIAN SEDIMENTARY BED-FORMS FROM RANDOM SURFACES

A Thesis

by

CHANDAN TANKALA

Submitted to the Office of Graduate Studies of
Texas A&M University
in partial fulfillment of the requirements for the degree of

MASTER OF SCIENCE

Approved by:

Co-Chair's of Committee,	Robert Weiss
	Michael Tice
Committee Member,	James Kaihatu
Head of Department,	John Giardino

August 2012

Major Subject: Geophysics

ABSTRACT

Numerical Analysis on the Generation of Equilibrium Aeolian Sedimentary Bed-forms from Random Surfaces. (August 2012)

Chandan Tankala, B.Tech, National Institute of Technology, India

Co-Chair's of Advisory Committee: Dr. Robert Weiss
Dr. Michael Tice

The formation of aeolian ripples have been modeled, quite successfully, using discrete approaches like cellular automaton models. Numerical analysis of continuum models to obtain similar success in modeling ripple evolution, however, has not been studied extensively. A numerical model based on continuum theories expedites calculations , as opposed to discrete approaches which model trajectory of each and every sand grain, and are hence relatively more economical. The numerical analysis strives to contribute to the field of study of aeolian ripple migration by an extensive comparison and discussion of modeled ripple evolution results with those of a particular laboratory based wind-tunnel experiment. This research also endeavors to understand the physics behind ripple generation and what parameters to be modified to account for multiple grain sizes. Incorporation of multiple grain sizes would enable us to study the stratigraphy of the generated bed-forms. To obtain smoother and realistic ripple surfaces, a sixth-order compact finite difference numerical scheme is used for spatial derivates and fourth-order Runge-Kutta scheme for time derivates. The boundary conditions incorporated are periodic and the initial condition employed to generate ripple is a rough sand surface. The numerical model is applied to study the effect of varying the angle, at which the sand bed gets impacted by sand grains, on the evolution of ripples. Ripples are analyzed qualitatively and quantitatively by considering the contribution of processes involved in the evolution process. The ripple profiles and the time taken to reach equilibrium state, obtained by numeri-

cal experiments, are in close agreement with the ones obtained by the wind-tunnel experiment.

TABLE OF CONTENTS

Page

LIST OF TABLES

LIST OF FIGURES

FIGURE Page

FIGURE Page

FIGURE Page

1. INTRODUCTION

1.1 Overview

Aeolian ripples can be found in deserts, geologic record of aeolian sandstones and lately have also been found on Mars. The scale of wavelength of these ripples can range from a centimeters to meters and correspondingly amplitudes from millimeters to centimeters (Yizhaq et al., 2004). The study of these features enables us to comprehend the environmental conditions that produced them. Although wind energy is required for the formation of ripples, the saltation of grains and the evolution is self-organizational. Hence it is imperative to study how such a process generates impressive ripple patterns observed in deserts, etc.

This research endeavors to analyze the physics and the spatial, temporal scales at which the aeolian bed-forms are generated from initial random sand surface. An analytical aeolian sediment transport model (Hoyle and Mehta, 1999) is modeled numerically so as to understand how the analytical model relates to the actual physical processes behind aeolian sediment transport and the spacial, temporal scales at which these processes occur. The analytical model developed by Hoyle and Mehta (1999) is a continuum model and is solved numerically by implementing a compact finite difference scheme for the derivates. Progression of research in the field of aeolian sediment transport is described in the following section.

1.2 Aeolian sediment transport

Wind blowing over a sand bed causes sand to re-organize and develop wave-like patterns (Anderson, 1990). These wave-like patterns can occur at two major scales of length which we commonly know as ripples and dunes. Fig. 1.1 shows an example of a steady-state ripple pattern engraved on a aeolian sand bed. It is outside the

This thesis follows the style of *Geophysics*.

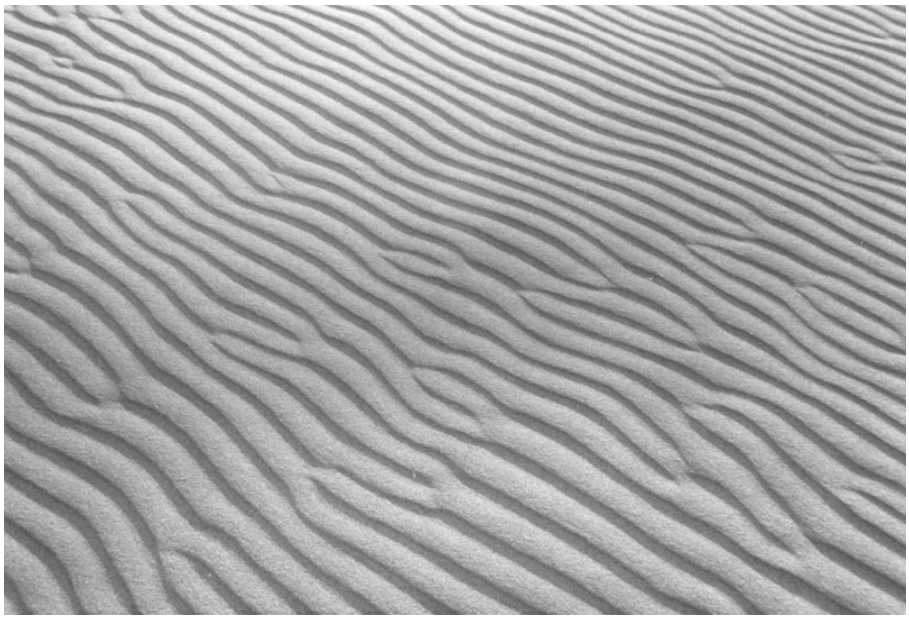

Fig. 1.1.: A ripple field in North Panamint Dunes, eastern California (Anderson, 1990). The sand in this field is well sorted (D=0.3 mm) and the ripples have a common equilibrium wavelength of approximately 8 cm.

scope of this research to study dunes but scientific inquiry about the physics behind the formation of aeolian ripples is very much the objective of this research. Ripples usually have wavelengths of a few centimeters and the ratio of height to length of the ripples commonly ranges from 1:15 to 1:20 (Hoyle and Woods, 1997).

During the very early period of research on aeolian ripples, it was believed that a sand bed buckles as a whole, behaving like a highly viscous fluid, and results in the formation of ripples. In 1941, Bagnold put forth a completely different perspective on understanding the formation of aeolian ripples. According to Bagnold (1941), it is the interaction between grains, on a sand surface, which is responsible for the formation of ripples. Bagnold (1941) introduced the concept of impacting grains which are highly energetic, referred to as saltating grains, and argued that the length these gains saltate is related to the wavelength of the ripples which we witness in nature. Although Bagnold addressed the rolling of grains, caused as a result of saltation, he did not discuss the role of rolling grains in the evolution of ripples.

In the years to follow, Bagnold's theory was challenged by many theories of which Sharp (1963), Seppala and Linde (1978) were the eminent ones. According to Sharp (1963), it is the ripple's amplitude and the angle of saltation which affect ripple wavelength rather than the length of saltation as proposed by Bagnold (1941). Sharp (1963)'s theory was based on his argument that ripple wavelength is controlled by the length of the side of the ripple which is not impacted by saltating grains (referred to as "shadow-zone"), which in turn depends on the amplitude of the ripple. Sharp (1963) disproved Bagnold (1941)'s theory by specifying that the generation of equilibrium state of ripples which have higher wavelength and amplitude than the initial ones from which they are produced over time cannot be be explained by influence of saltation length but can be explained by the influence of "shadow-zone". Seppala and Linde (1978) calibrated the ripple wavelength as it evolved with time by conducting wind tunnel experiments discussed later in subsection "Wind-Tunnel Experiments".

Later, Anderson (1987) proposed a theory that the saltation grains collide with the sand bed and transfer momentum to the bed, causing the ejection of other saltating grains and grains with low energy which tend to roll on the sand surface. These grains, referred to as reptating grains, are believed to be responsible for the evolution and the shape of ripples (Anderson, 1990). Thus, Anderson argued that wind is not directly responsible in shaping up the ripple surface and in fact does not play a major role in deciding the saltation lengths of the grains. Therefore, Anderson (1990) suggested that the asymptotic wavelength of the ripples does not depend on the wind energy function and the whole evolution process is self-organizational. The interaction between the saltating and reptating grains has been accounted for by the introduction of a new function, referred to as "Splash-function", in Anderson (1990).

Cellular Automaton (CA) models, e.g. Werner and Gillespie (1993); Landry and Werner (1994), described in detail later, have been extensively used to model the dynamics of ripples. The CA models, along with wind-tunnel experiments, have proven

effective in modeling how grains of different sizes segregate and also the stratigraphy of the bed-forms seen in the field during ripple evolution (Baas, 2007). Concurrently, continuum models, e.g. Nishimori and Ouchi (1993); Hoyle and Mehta (1999); Yizhaq et al. (2004), based on self-organisation (Anderson, 1990) and other analytical approaches, based on reducing the complex phenomenon of ripple formation into separate interacting processes, have also been more or less equally successful. Both CA and continuum models have their own advantages and disadvantages and are discussed in detail later.

1.3 Research objectives

The objective of this research is to numerically solve the empirical equations of aeolian sediment transport developed by Hoyle and Mehta (1999) so as to comprehend the contribution of different physical processes responsible in the evolution of sand bed and to analyze the spacial and temporal scale of the ripples obtained by results of the implemented numerical model. The numerical model is programmed in FORTRAN (computer programming language) using a sixth-order compact finite difference scheme for spacial derivatives and a fourth-order Runge-Kutta scheme for time derivatives. Specific objectives are detailed below:

1.3.1 Objectives

1. To study the length of the time required to produce an equilibrium bed form surface, if it exists at all, under steady-state conditions

2. To analyze the skill of Hoyle and Mehta (1999)'s model in reproducing the ripple parameters as measured by laboratory based wind-tunnel experiments

3. To interpret the contribution of each physical process towards the generation of bed-forms by looking at the relative contribution of the terms of the equations which correspond to the respective physical processes

2. BACKGROUND

2.1 Wind tunnel experiments

Although aoelian ripples have been studied by various models over the years, only a few controlled experiments have been conducted. This section discusses two important experiments and the progress made over the years in wind-tunnel tunnel experiments to better understand the evolution and steady state of ripples. Seppala and Linde (1978), have conducted a wind-tunnel experiment to study ripple formation with changing wind velocities and time. The wind-tunnel chosen was a recirculating one and had dimensions of 0.6 × 0.6 × 4.0 m. The experiment setup could vary speed of wind anywhere between $2ms^{-1}$ and 14 ms^{-1} (Seppala and Linde, 1978). Well sorted sand was used and Fig. 2.1 shows the structure of the wind tunnel.

There seems to be a minimum wind velocity required for the formation of ripples which depends on the shear velocities required for grains to be ejected from their stationary positions. A large number of ripples of smaller height and length are observed at lower wind velocities and larger ripples at higher wind velocities.

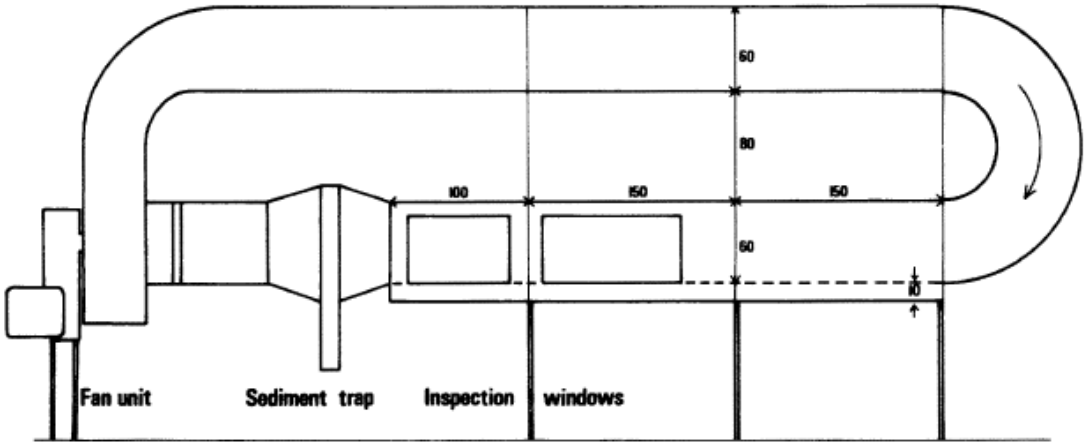

Fig. 2.1.: Design of wind tunnel used by Seppala and Linde (1978). Numbers indicate length in cm. The direction of wind is shown by arrows.

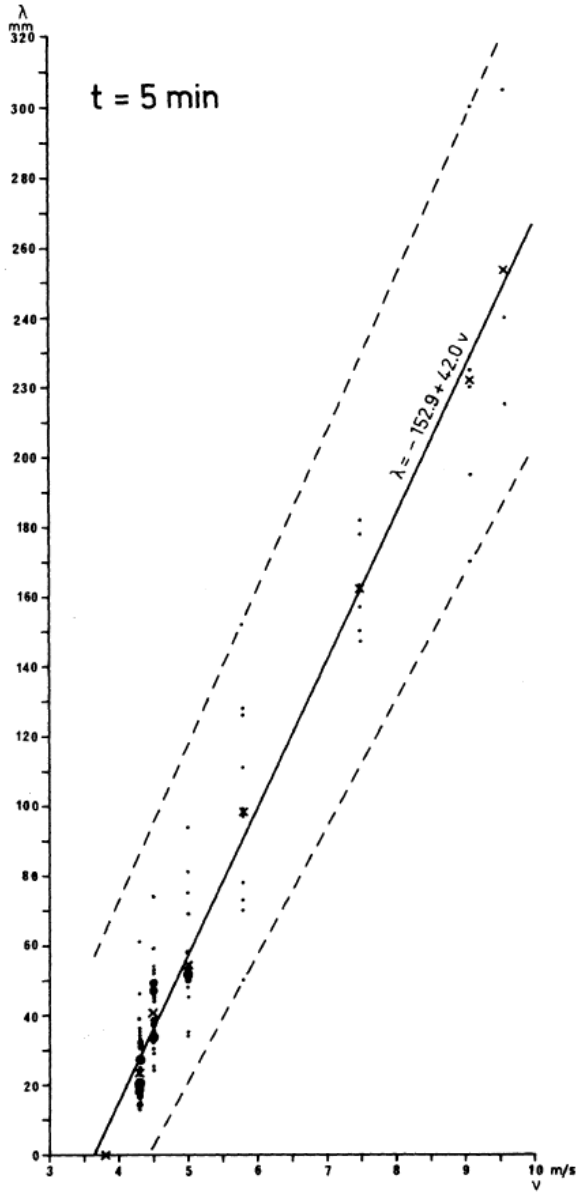

Fig. 2.2.: Wavelength of ripples against speed of wind used in the experiments. Experiments are run for 5 mins. The equation of the straight line is constructed based on average values of ripple wavelength (shown by crosses) with the co-relation coefficient being 0.998 (Seppala and Linde, 1978).

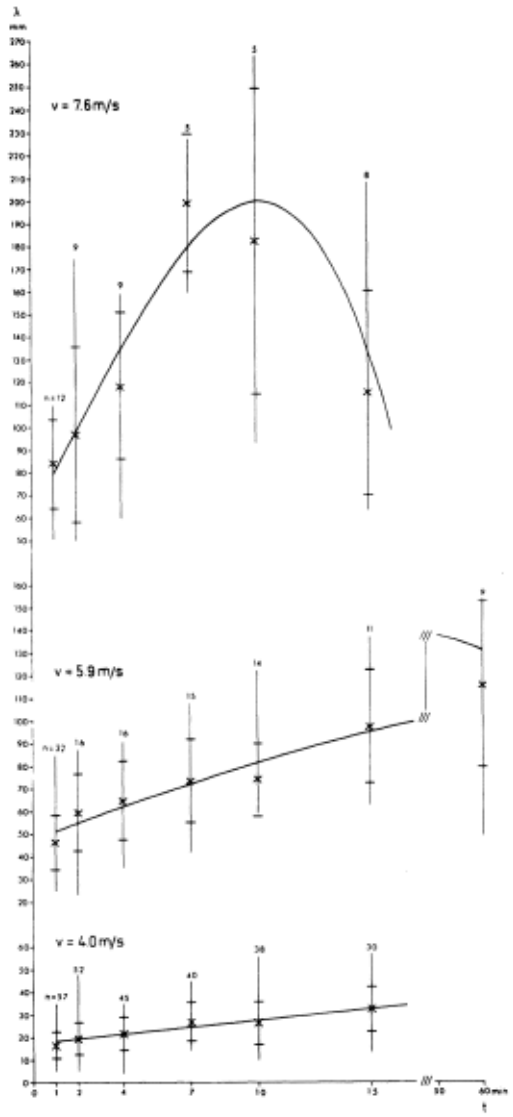

Fig. 2.3.: Wavelength of ripples versus time-period of an experimental run for changing speeds of wind ("v" stands for the speed of wind). The construction of curves is based on average values of wavelength shown by crosses (Seppala and Linde, 1978).

Fig. 2.2 depicts a nearly linear rate of increase of wavelength of the ripples with wind velocities for the same run time of 5 mins.

Fig. 2.3 shows that at lower wind velocities, there is a nearly linear rate of increase in the wavelength of the ripples with run-time of the experiment. But, at higher velocities there seems to be a steep increase in the ripple wavelength during initial times and then an equally steep decrease in the wavelength. According to the authors, during the initial times the ripple height and wavelength increase as expected and reach a point beyond which grains from the ripple crest wear away into the following trough before an ensuing ripple is formed (Seppala and Linde, 1978).

Since the wind tunnel experiment described above, various other controlled experiments have been conducted to study aeolian ripples in the non-linear regime. Although Seppala and Linde (1978), described fully developed ripples they were not studied in detail. It is commonly predicted that the wavelength of the ripples increases with run-time continuously. Experiments need to be developed which inspect the conditions responsible for generating a steady-state of ripples beyond which ripples do not evolve in shape and size. Andreotti et al. (2006) made significant headway in understand the aforementioned conditions and conducted an extensive investigation of the geometries aeolian sand ripples in steady-state both in a wind tunnel and on the leeward side of a dune.

The wind tunnel used by Andreotti et al. (2006) has dimensions of 4.5 m $\times$ 1 m $\times$ 0.5 m, and the sand used is angular in shape. On the other hand, grains used in the dune field experiment are relatively more smooth. The two main objectives of this study were to study the saturated states beginning from a flat sand surface and from a nearly flat but random sand surface. Fig. 2.4(a) and (b) show the evolution of ripples with time, both in the wind tunnel and in the dune field, from an initial flat surface of sand. It is observed that in both of these cases, the initial surface gets disturbed with the formation of very small ripples and eventually bigger ripples, in terms of wavelength and height, are formed. Fig. 2.4(c) indicates that although there is an increase in the wavelength initially, the growth in wavelength decreases with time and a stage of saturation is attained where is there is no or very little growth in

wavelength. Similar trends are observed for the amplitudes of these ripples as shown in Fig. 2.4(d).

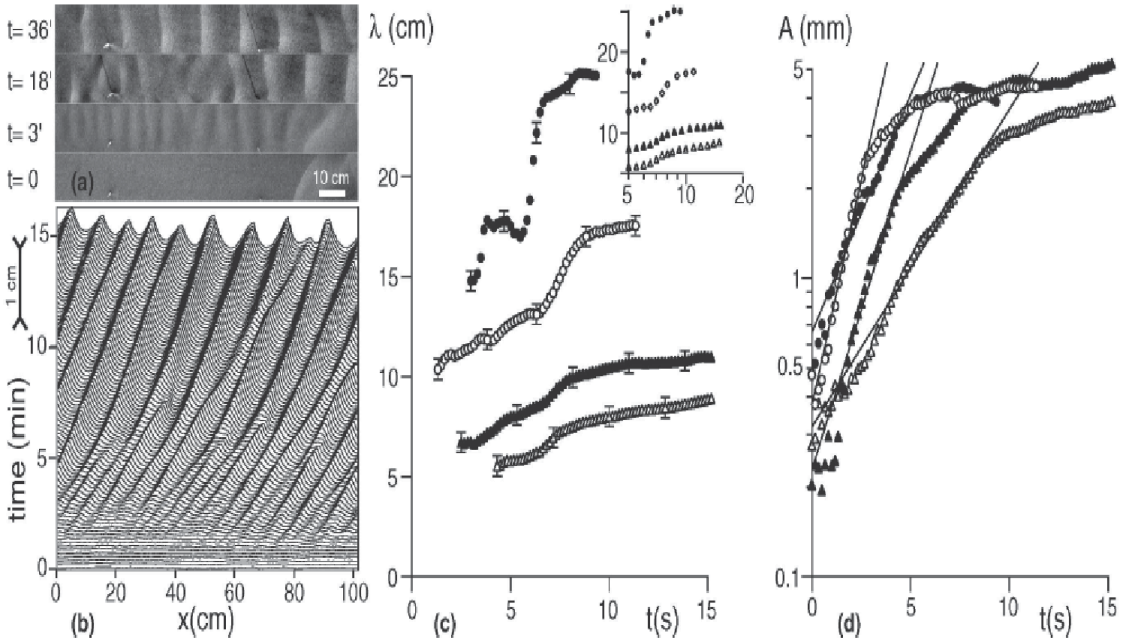

Fig. 2.4.: Transformation of a flat surface of sand with time both in the wind-tunnel and in the dune field (a) Snapshots of a dune field at different times for wind shear speed $u^* = 1.3u_{th}$ (b) Ripple profile, in the wind-tunnel, along space and time domain for wind-shear speed $u^* = 1.4u_{th}$ (u_{th} stands for critical saltation speed) (c) Plot of wavelength of ripples against time (time in the inset graph is in log scale) for multiple wind-shear speeds (d) Plot of amplitude of ripples against time for multiple wind-shear speeds $u^* = 1.3u_{th}(\Delta)$, $u^* = 1.4u_{th}(\blacktriangle)$, $u^* = 1.8u_{th}(\circ)$, $u^* = 2.3u_{th}$ $(\bullet)$(*Andreottiet al.*, 2006)

The other part of the study by Andreotti et al. (2006) was to study ripples formed from an initially disturbed sand bed. For this purpose, a periodic ripple chain on the bed of sand was setup as an initial condition. Fig. 2.5 describes the evolution with time similar to Fig. 2.4. It has been observed that if the initial wavelength of the ripples is equal to that of the steady-state wavelengths obtained from a flat sand surface, then ripples simply migrate without a change in the wavelength and amplitude as seen Fig. 2.5(b) and (e). If the initial wavelength is significantly smaller or larger

than the saturation wavelength, then either ripples merge or diffuse respectively and reach a saturated stable ripple profile shown in Fig. 2.5(d) and (f).

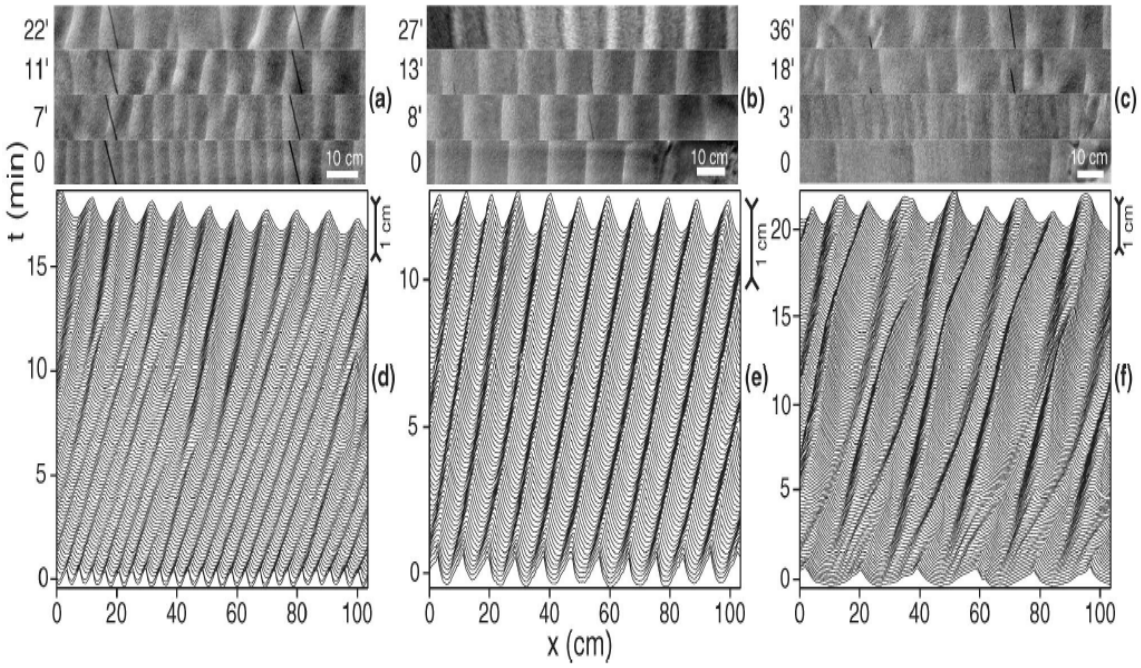

Fig. 2.5.: Transformation of a random surface of sand with time both in the wind-tunnel and in the dune field. Snapshots of a dune field at different times for wind-shear speed $u^* = 1.3u_{th}$ beginning with a wavelength of (a) λ=5 cm; (b) λ=13.5 cm; (c) λ=30 cm. Ripple profile, in the wind-tunnel, along space and time domain for for wind-shear speed $u^* = 1.3u_{th}$ beginning with a wavelength of (a) λ=5 cm; (b) λ=9.3 cm; (c) λ=19.5 cm (Andreotti et al., 2006)

Fig. 2.6 shows how relative amplitude and wavelength play a role in reaching a stable ripple profile depending on the initial bed surface. If the experiment is begun with the saturation wavelength but with a marginally (+/- 5 cm) different amplitude, ripples develop in a way that the amplitude eventually gets adjusted to the saturation amplitude. But, if the experiment is begun with the saturation amplitude with a marginally different wavelength, then ripples preserve this initial wavelength and evolve into a stable and new amplitude. Thus, it can be concluded

that a range of stable saturated ripple states can exist all of which depend on the initial conditions.

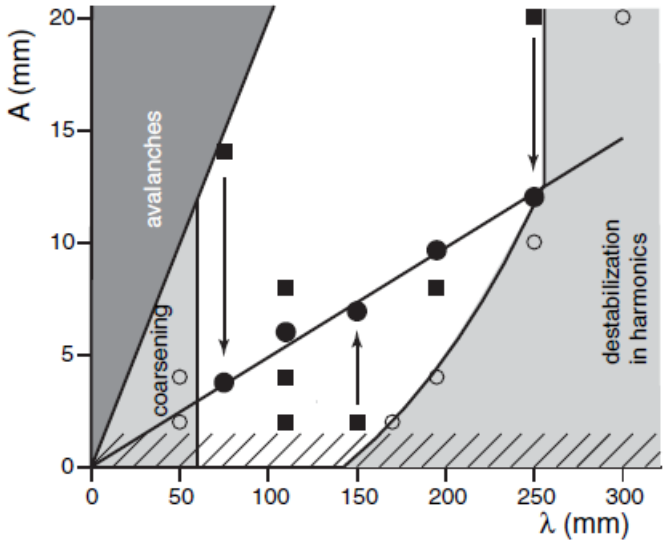

Fig. 2.6.: Amplitude (A) vs Wavelength (λ) relationship diagram spanning from initial state to steady state for wind-shear speed $u^* = 1.3u_{th}$ (Andreotti et al., 2006). (●) indicates stable wavelength-amplitude combinations and (■) indicates initial wavelength-amplitude combinations. Arrows show the direction from the initial state to the stable state. The zone outside the (○) and the hatched region are beyond the scope of this research.

2.2 Continuum and discrete models

Over the past two decades, during which a many studies have been published on numerical modeling of aeolian ripples, scientists have adopted ideologically different approaches for modeling aeolian ripple migration. One of the approaches is to formulate a discrete numerical method which basically meshes the sediment bed using appropriate shapes and assign properties to each element of this mesh. The properties that can be included are random sand grain interaction behavior which are erosional or depositional of nature. Cellular automaton modeling is the most popular

method among the discrete numerical methods. Although these models can accommodate an array of grain sizes, can help understand the stratigraphy and how grains segregate during the evolution of ripples, they lack the basis of collisional dynamics which are responsible for ripple migration and evolution (Yizhaq et al., 2004). On the other hand, continuum models are based on deriving equations for transport of a local mass of sediment (Anderson, 1987; Sauermann et al., 2001) based on the actual physical processes that occur. Hence continuum models give a better understanding of the contribution of different processes involved in the time evolution of ripples.

2.2.1 Cellular automaton models

One of the earliest cellular automaton simulation models was the one developed by Forrest and Haff (1992). This model simulated the path of every moving sediment particle. In this model, ripples with a significant difference in size were not observed because ripples with a little difference in size merge as their windward and leeward side zones overlap causing swapping of ripple speeds. Therefore, Forrest and Haff (1992) came to the conclusion that the development of steady state of ripples, beyond which ripples with do not grow in size and wavelength, is largely dependent on the merging of ripples over time. Werner and Gillespie (1993) introduced a new model to test the results produced by Forrest and Haff (1992). In the model by Werner and Gillespie (1993), ripples were represented as bars of different lengths. The migration of ripples was represented by the movement of these bars along a circular path (Werner and Gillespie, 1993). It is assumed that probability of movement of these bars decreases with an increase in the length of the bar. This allowed accounting for the merging of ripples but could not simulate the real dynamics and processes behind ripple merging.

Lately, Pelletier (2009) drew analogies between Werner (1995)'s dune dynamics model and ripple dynamics by scaling the dune size and roughness experienced by a dune because of wind to corresponding size and roughness experienced by a ripple.

Pelletier (2009) applied a correction to the speed with which higher amplitude ripples migrate arguing that these bigger bed-forms would be experiencing a higher shear stress than the one used by Werner (1995) model. Thus, with this increased speed with which ripples of higher amplitude move, Pelletier (2009) suggested that there smaller ripples would merge with a decreasing rate and thus allowing a steady state after which ripple wavelength does not change.

2.2.2 Continuum models

Anderson (1987)'s theory, as discussed in Introduction, was one of the first continuum models. Prigozhin (1999) furthered the work of Anderson (1987), introduced orginally by Bouchaud et al. (1994), to describe and account for the flux of rolling grains. Other models for rolling having been proposed by various authors and the one proposed by Hoyle and Mehta (1999) is a fairly good representation of the actual rolling process and hence the model by Hoyle and Mehta (1999) has been used in this research. Although there are major differences in implementing the rolling phase of grains, a majority of the continuum models seem to have a similar representation for saltation component. Saltation and reptation are discussed in detail in the next section.

2.3 Physical processes behind ripple migration

As described earlier, Anderson and Haff (1988) and Anderson (1990) had made a significant advance in understanding the physical processes involved and developing analytical models which describe the processes behind the evolution of ripples. A robust understanding of the saltation process has been accomplished by studying saltation path's in the 1980's (Jensen and Sorensen, 1986; Anderson and Hallet, 1986). It is now understood that highly energetic saltating grains eject grains on the sand bed in two ways as they collide the sand bed (Anderson, 1990). One of

those categories corresponds to those grains which have a speed of 1/2 to 1/3 of the impinging saltating grains and these grains continue saltation. The other category is the rolling grains whose speed is relatively less like 1/10 of the impinging saltating grains and may be referred to as reptating grains (Anderson, 1990). The process of sand grains beginning saltation because of the force exerted by excess shear speed of blowing wind, the trajectories of saltating grains, the grains ejected from the bed by these saltating grains, and the impact of the grains saltating on the wind regime have been simulated by Anderson and Haff (1988).

One of the analytical models of aeolian ripples which has been considered to be highly successful is by Hoyle and Mehta (1999). This model is an improvement over Anderson (1990) because, in addition to the transfer of energy between the grains in hopping and rolling phase, it also includes several other processes like diffusion and relaxation mechanisms which help produce smoother and realistic ripple surface profiles. This model and all other major subsequent continuum models compute a saltation flux and have representation of rolling and sliding. The processes are explained in detail in the following section.

2.3.1 Saltation or hopping

Wind causes sediment grains on the surface to hop with high speeds and impinge upon the sand surface at small angles. Speeds can be as high as 1 ms^{-1} (Anderson and Bunas, 1993) and the impact angles are commonly in the range of 10° -16°. Hoyle and Woods (1997) assumed that wind energy does not effect the saltation trajectories described by the probability function $p(a)$ based on the study by Jensen and Sorensen (1986) and since Hoyle and Woods (1997) developed their model for a single grain size, the angle of saltation is considered to be close to a constant. Hoyle and Woods (1997) assumed that the saltating grains continue in saltation after impacting the bed and do not stop. The grains ejected by the saltating grains,

described in earlier sections as reptating grains, roll with much lesser velocities and lengths than that of the saltating grains.

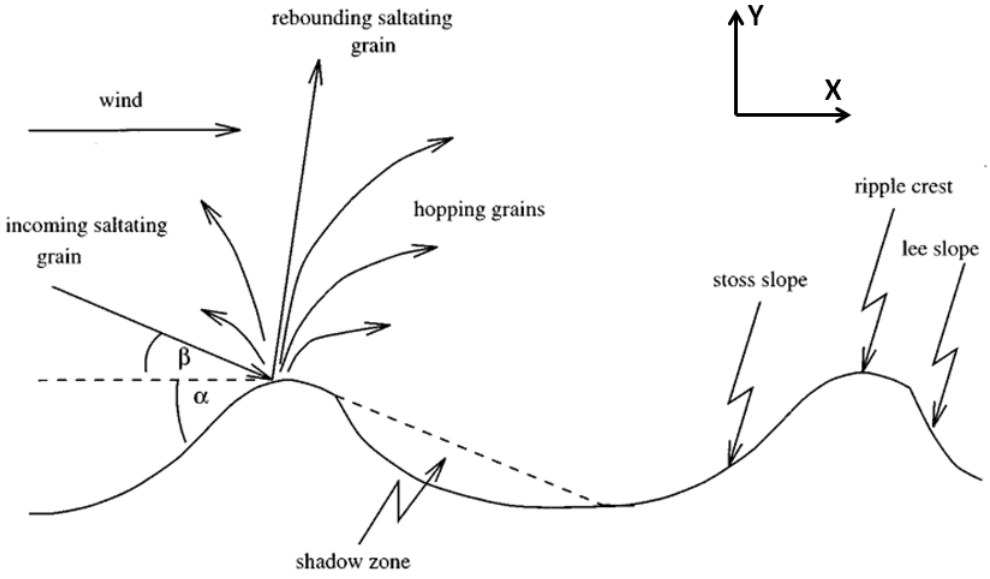

Fig. 2.7.: Description of saltation and reptation of sand grains (Hoyle and Woods, 1997)

$N(x,t)$ represents the number of sand grains that are set into the saltation phase per unit time and per unit length of the sand surface, at a point of co-ordinate x and at time t on a sand surface. According to Hoyle and Woods (1997), $N(x,t)$ is considered directly proportional to the normal component of incoming saltation flow at that point and hence

$$N(x,t) = J\sin(\alpha+\beta) \tag{2.1}$$

where J is a proportionality constant, α represents surface slope at that point and β the saltation angle with the horizontal at that point as shown in Fig. 2.7. The distance traversed horizontally a by the grains which continue in saltation is described by a probability distribution function $p(a)$ (Hoyle and Woods, 1997; Hoyle and Mehta, 1999), where

$$\int_{-\infty}^{\infty} p(a)da = 1 \tag{2.2}$$

If $\delta n(x,t)$ represents the difference between the number of grains that land by saltation and the number of grains that leave by saltation between co-ordinates x and $x + \delta x$ within time δt, then (Hoyle and Woods, 1997):

$$\delta n(x,t) = \int_{-\infty}^{\infty} p(a)\left[N(x,t) - N(x-a,t)\right] da\delta x\delta t \tag{2.3}$$

Because of conservation of mass, the amount of change in height $y(x,t)$ of the surface of sand, in time δt, is evaluated by (Hoyle and Woods, 1997):

$$\delta x\delta y(x,t) = a_p\delta n(x,t) \tag{2.4}$$

where a_p represents a single sand grain's mean area of cross-section. The rate of change of height of the sand surface can be obtained by integrating the above two equations and thus leading to (Hoyle and Woods, 1997):

$$\frac{\partial y}{\partial t}(x,t) = -a_p \int_{-\infty}^{\infty} p(a)\left[N(x,t) - N(x-a,t)\right] da \tag{2.5}$$

Hoyle and Woods (1997) evaluated the integral using Taylor's series and ignored the second-order terms of the Taylor's series, by assuming the second-order terms to be

very small compared to the first-order terms, the equation for rate of change of height of sand surface, caused by hopping alone, is given by (Hoyle and Woods, 1997):

$$\frac{\partial y}{\partial t}(x,t) = -Ja_p\bar{a}\frac{\partial^2 y}{\partial x^2}\frac{(\cos\beta - \sin\beta(\frac{\partial y}{\partial x}))}{1+(\frac{\partial y}{\partial x}^2)^{3/2}} \tag{2.6}$$

2.3.2 Rolling

As the sand bed re-organizes as a result of reptation caused by saltation, some grains roll down because of gravity. There exists a critical slope on the sand bed beyond which this rolling occurs referred to as the angle of repose. Angle of repose is a function of the way sand is packed and is usually around 30° (Hoyle and Woods, 1997). In addition to the this angle of repose, Hoyle and Woods (1997) defined another angle referred to as "dynamic angle of repose" γ and proposed that if the slopes reach dynamic angle of repose, then slope failure occurs and the grains run down as an avalanche instead of rolling. Hoyle and Woods (1997) assumed that as the sand slope reaches γ, slope fails by an avalanche and that the grains fall down in a way that the angle of slope remains constant at the angle γ.

At smaller sand surface slopes (less than $\tan\gamma$), Hoyle and Woods (1997) assumed that the sand particles roll down with a constant velocity u, which is given by:

$$u = -\frac{g}{r}\sin\alpha = -\frac{g}{r}\frac{\frac{\partial y}{\partial x}}{\left[1+\left(\frac{\partial y}{\partial x}\right)^2\right]^{1/2}} \tag{2.7}$$

where r is the frictional coefficient between the grains and this is assumed to be a constant by Hoyle and Woods (1997). The flux of sand grains which roll horizontally $Q(x,t)$ is considered proportional to the above calculated rolling velocity by Hoyle and Woods (1997). Hence,

$$Q(x,t) = -F\frac{g}{r}\sin\alpha\cos\alpha = -F\frac{g}{r}\frac{\frac{\partial y}{\partial x}}{\left[1+\left(\frac{\partial y}{\partial x}\right)^2\right]} \tag{2.8}$$

where F is a proportionality constant. The problem of avalanching, which occurs at slopes close to $\tan\gamma$, has been addressed by (Hoyle and Woods, 1997):

$$Q(x,t) = -F\frac{g}{r}\tan^2\gamma \times \frac{\frac{\partial y}{\partial x}}{\left[1+\left(\frac{\partial y}{\partial x}\right)^2\right]\left[\tan^2\gamma - \left(\frac{\partial y}{\partial x}\right)^2\right]^{1/2}} \tag{2.9}$$

and the rate of change of sand bed surface height is given by:

$$\frac{\partial y}{\partial t} = -a_p\frac{\partial Q}{\partial x} \tag{2.10}$$

where a_p represents a single grain's average size. The rate of change of sand surface height, caused by rolling alone, is given by combining the above two equations (Hoyle and Woods, 1997):

$$\frac{\partial y}{\partial t} = D\frac{\partial^2 y}{\partial x^2} \tag{2.11}$$

where

$$D = F(\tan^4\gamma)a_p\frac{g}{r}\frac{1-(\frac{\partial y}{\partial x})^2}{[1+(\frac{\partial y}{\partial x})^2]^2[\tan^2\gamma - (\frac{\partial y}{\partial x})^2]^{1/2}}$$

3. ANALYTICAL DESCRIPTION

3.1 Governing equations

An aeolian sediment transport model that incorporates all the significant phenomenon responsible for aeolian transport and hence the formation and migration of ripples, described in the section "Background", have been described empirically by Hoyle and Mehta (1999). The governing equations for the height of sand bed $h(x,t)$ and the density of sand grains $\rho(x,t)$ with time, in Hoyle and Mehta (1999)'s model, at varying sand surface slopes are as follows:
If $0 \leq h_x \leq \frac{\tan\alpha}{\tan\gamma}$, then

$$h_t = (1+\hat{\kappa}\rho)h_{xx} - \rho\frac{\tan\beta}{\tan\alpha}(|h_x| - \frac{\tan\alpha}{\tan\gamma}) - f(x) \tag{3.1}$$

$$\rho_t = \frac{h_0}{\rho_0}(-\hat{\kappa}\rho h_{xx} + \rho\frac{\tan\beta}{\tan\alpha}(|h_x| - \frac{\tan\alpha}{\tan\gamma})) + \frac{h_0}{\rho_0}\int_{-\infty}^{\infty} p\,(a)\,f\,(x-a)\;da + \frac{D_\rho}{D_h}\rho_{xx} + \hat{\chi}\,(\rho h_x)_x \tag{3.2}$$

and if $\frac{\tan\alpha}{\tan\gamma} \leq h_x \leq 1$, then

$$h_t = (1+\hat{\kappa}\rho)h_{xx} - \frac{\hat{v}(|h_x| - \frac{\tan\alpha}{\tan\gamma})}{(1-h_x^2)^{1/2}} - f(x) \tag{3.3}$$

$$\begin{aligned}\rho_t = \frac{h_0}{\rho_0}(-\hat{\kappa}\rho h_{xx} + \frac{\hat{v}(|h_x| - \frac{\tan\alpha}{\tan\gamma})}{(1-h_x^2)^{1/2}}) \\ + \frac{h_0}{\rho_0}\int_{-\infty}^{\infty} p(a)f(x-a)\,da + \frac{D_\rho}{D_h}\rho_{xx} + \hat{\chi}(\rho h_x)_x\end{aligned} \tag{3.4}$$

$$f(x) = (h_x + \frac{\tan\beta}{\tan\gamma})[1 + {h_x}^2 \tan\gamma^2]^{-1/2} \tag{3.5}$$

D_ρ and D_h are positive coefficients of diffusion. The description of all the constants and derivation of these equations is given in the subsequent section.

3.2 Justification for Hoyle and Mehta (1999)'s model

Although Anderson (1990) was the first to introduce the importance of the reptation phase in the development of bed-forms by means of a "splash" function, it was based on several assumptions, one of which was that the splash function was independent of the angle of saltation. This would have an impact in the results because there would be a difference in the exchange of momentum between lower angles of saltation against higher angles of saltation. This error in momentum exchange effects the velocities and angles with subsequent grains get saltated. Improvements were made in future years in understanding the reptation phase. Bouchaud et al. (1994) introduced the concept of avalanche flows and Hoyle and Mehta (1999) came up with a better model for rolling as discussed in background. Hoyle and Woods (1997)'s one-species continuum model incorporated models for all the processes namely saltation, hopping, rolling and avalanching.

Then, (Hoyle and Mehta, 1999) proposed an improvement over the Hoyle and Woods (1997) model by incorporating the processes responsible for diffusion of both the group of grain in saltation and in reptation referred to as "relaxations effects" by Hoyle and Mehta (1999). This diffusion was implemented both within the groups of grains and between the groups of grains which significantly improved ripple surface profiles. The model by (Hoyle and Mehta, 1999) also allowed calculation of wavelength of the ripples and speed with which they propagate (which the previous models could not come up with explicitly).

3.3 Presentation of Hoyle and Mehta (1999)'s model

This model has drawn analogies from sand piles by accommodating "bistability" at the angle of repose which the Hoyle and Mehta (1999) believe has an important effect on the evolution of ripples. Hoyle and Mehta (1999) define bistability as the nature of sand to be either stable (at rest) or be flowing at slopes of the sand surface above the angle of repose. The maximum angle above the angle of repose beyond which sand can no longer be stable is defined as the maximum angle of stability γ (Hoyle and Mehta, 1999). Beyond the maximum angle of stability γ, avalanching occurs rapidly.

The height of the sand surface at a point with horizontal co-ordinate x at time t is defined as $h(x,t)$ and similarly the density of flowing grains as $\rho(x,t)$. The sand surface is subjected to a constant saltation flux at an angle β to the horizontal which eject both saltating and reptating grains and then the relaxation mechanisms come into play and create a smooth ripple surface on sand. α is the angle of repose. The differential equations for $h(x,t)$ and $\rho(x,t)$ are described in equations 3.1- 3.4. The derivation of these equations is similar to that of the Hoyle and Woods (1997)'s model and is described below:

If $N(x,t)$ represents the number of sand grains that are set into saltation phase per unit length of sand bed and per unit time, then $N(x,t)$ is considered directly proportional to the normal component of the incoming flow of saltation at that point (Hoyle and Mehta, 1999):

$$N(x,t) = J\sin(\alpha+\beta) = \frac{J(\sin\beta + h_x\cos\beta)}{(1+h_x^2)^{1/2}} \tag{3.6}$$

where J is a proportionality constant and $\tan\alpha = (h_x)$

The trajectories of saltating grains is described by a probability distribution function $p(a)$ where a sand grain has a probability of $p(a)$ to saltate a distance a along the horizontal direction. Hoyle and Mehta (1999) considered the duration of hop

of a grain to be negligible compared to the duration of the evolution of ripples. If $\delta n_0(x,t)$ represents the number of grains on the surface of sand between co-ordinates x and $x+\delta x$ that are set into saltation within time dt, then as per the definition of $N(x,t)$ (Hoyle and Mehta, 1999):

$$\delta n_0(x,t) = N(x,t)\delta x \delta t \tag{3.7}$$

If a_p represents a single grain's mean area of cross-section, then the area of grains on the surface of sand between co-ordinates x and $x+\delta x$ that are set into saltation is $a_p \delta n_0(x,t)$ which is also equal to $-\delta x \delta h(x,t)$ (Hoyle and Mehta, 1999). Hence,

$$a_p \delta n_0(x,t) = -\delta x \delta h(x,t) \tag{3.8}$$

Derivative of $h(x,t)$ can be defined by supposing $\delta t \to 0$, and hence the change of the surface height caused by saltation alone is (Hoyle and Mehta, 1999):

$$h_t = -a_p N(x,t) = -a_p J \frac{\sin\beta + h_x \cos\beta}{(1+h_x^2)^{1/2}} \tag{3.9}$$

Of the windward and the leeward side of a ripple, the sand grains on the leeward side are not ejected by the saltation flux and hence the points on this side do not contribute towards the h_t equation described above. If $\delta n(x,t)$ represents the number of saltating grains that land between co-ordinates x and $x+\delta x$ on the sand surface within time δt (Hoyle and Mehta, 1999), then:

$$\delta n(x,t) = \int_{-\infty}^{\infty} p(a) N(x-a,t) da \delta x \delta t \tag{3.10}$$

According to conservation of mass,

$$\delta x \delta \rho(x,t) = a_p \delta n(x,t) \tag{3.11}$$

Hence by combining equation 3.10 and equation 3.11, the change in the surface density of grains with time, by saltation alone, is given by (Hoyle and Mehta, 1999):

$$\rho_t = a_p J \int_{-\infty}^{\infty} p(a) \frac{\sin\beta + h_x(x-a,t)\cos\beta}{[1+h_x^2(x-a,t)]^{1/2}} da \tag{3.12}$$

Hoyle and Mehta (1999) adopted the processes which account for energy transfer between the hopping grains and the group of grains which are in the rolling phase by including transfer terms. In addition to this, Hoyle and Mehta (1999) also included diffusive motion and computed h_t and ρ_t shown in equations 3.13 and 3.14.

$$h_t = D_h h_{xx} - T(x,t) - a_p J \frac{(\sin\beta + h_x \cos\beta)}{(1+h_x^2)^{1/2}} \tag{3.13}$$

$$\rho_t = D_\rho \rho_{xx} + \chi(\rho h_x)_x + T(x,t) + a_p J \int_{-\infty}^{\infty} p(a) \frac{\sin\beta + h_x(x-a,t)\cos\beta}{[1+h_x^2(x-a,t)]^{1/2}} da \tag{3.14}$$

where

1. D_ρ and D_h are positive coefficients of diffusion
2. κ, χ are positive constants
3. $T(x,t)$ represents terms which stand for energy transfer between the hopping grains and group of grains in rolling phase
4. $p(a)$ represents the probability distribution function with which grains saltate a horizontal distance 'a'

The value of $T(x,t)$, at different surface slopes, is described in equations 3.15 and 3.16 (Hoyle and Mehta, 1999):

For $0 \leq |h_x| \leq \tan\alpha$,

$$T(x,t) = -\kappa\rho h_{xx} + \lambda\rho(|h_x| - \tan\alpha) \tag{3.15}$$

and for $\tan\alpha \leq |h_x| \leq \tan\gamma$,

$$T(x,t) = -\kappa\rho h_{xx} + \frac{\upsilon(|h_x| - \tan\alpha)}{(\tan^2\gamma - h_x^2)^{1/2}} \tag{3.16}$$

where υ is a constant which is positive. The diffusion of the group of grains that are in rolling phase and those in saltation are represented by $D_h h_{xx}$ and $D_\rho \rho_{xx}$ respectively. $\chi(\rho h_x)_x$ represents the the motion of grains on the bed caused by gravitational forces. According to Hoyle and Mehta (1999), the excessive extrusions on the crests or ditches on the troughs of ripples would be removed or filled out by rolling grains which is represented by $-\kappa\rho h_{xx}$. If the slopes are not steep enough, i.e. for slopes less than $\tan\alpha$, then the rolling grains would tend to adhere to the surface of the ripple or roll at smaller speeds represented by the term $\lambda\rho(|h_x| - \tan\alpha)$. The grains on the slopes less than $\tan\alpha$, thus, do not get ejected because of saltation flux. But at slopes greater than $\tan\alpha$, grains on the ripples tend not to be stable and are prone to avalanching which is modeled by the term $\upsilon(|h_x| - \tan\alpha)(\tan^2\gamma - h_x^2)^{-1/2}$. This tendency increases with the value of slope and as the slopes approach $\tan\gamma$, avalanching occurs instantaneously (Hoyle and Mehta, 1999).

The equation's 3.13 and 3.14 are non-dimensionalized by substituting $x \rightarrow x_0\tilde{x}$, $t \rightarrow t_0\tilde{t}$, $a \rightarrow x_0\tilde{a}$, $h \rightarrow h_0\tilde{h}$, $\rho \rightarrow \rho_0\tilde{a}$ (Hoyle and Mehta, 1999). The final analytical equations for h_t and ρ_t (equations 3.1, 3.2, 3.3, 3.4), at different slopes, are thus obtained by ignoring the tildes and where the values of non-dimensionalization constants are described in Table 3.1 (Hoyle and Mehta, 1999).

Table 3.1: Non-dimensionalization constant values

Constant	Values
$h_0 =$	$\frac{D_h \tan\gamma}{a_p J \cos} \beta$
$\rho_0 =$	$\frac{a_p J \sin\beta}{\tan\alpha}$
$x_0 =$	$\frac{D_h}{a_p J \cos\beta}$
$t_0 =$	$\frac{D_h}{(a_p J \cos\beta})^2$
$\hat{\kappa} =$	$\frac{\kappa\rho_0}{D_h}$
$\hat{\mu} =$	$\frac{\mu t_0}{h_0}$
$\hat{\chi} =$	$\frac{h_0}{D_h}$

The term $f(x)$, in the equations 3.1 and 3.3, represents the contribution to the rate of change of height caused by saltation of the grains alone. These saltating grains landing into the rolling group of grains is represented by this analytical term: $\int_{-\infty}^{\infty} p(a) f(x-a)\, da$. Thus $f(x)$ is not used in the h_t equation for points on the leeward side of the ripples because they do not get impacted by saltation flux.

4. NUMERICAL EXPERIMENTS

4.1 Description of numerical model

A compact finite difference scheme has been used to numerically model the equations 3.1- 3.4 in FORTRAN programming language. The compact finite difference scheme has been used for space derivates and a Runge-Kutta fourth order scheme for time derivates in equations 3.1- 3.4. The finite differencing scheme for the derivates is implemented by dividing space domain into parts of equal spacing $\delta x = x_i - x_{i-1}$ and similarly time domain into parts of equal spacing $\delta t = t_i - t_{i-1}$. The compact finite difference represents a sixth-order calculation formula for the spatial derivates and less associated truncation errors (Gamet et al., 1999). First and second derivatives of a random function g with respect to x, at any point k, using this finite difference scheme, are as follows (Gamet et al., 1999):

$$\frac{1}{3}g'_{i-1} + g'_i + \frac{1}{3}g'_{i+1} = \frac{14}{9}\frac{g_{k+1} - g_{k-1}}{2\delta x} + \frac{1}{9}\frac{g_{k+2} - g_{k-2}}{4\delta x} \tag{4.1}$$

$$\frac{2}{11}g''_{i-1} + g''_i + \frac{2}{11}g''_{i+1} = \frac{12}{11}\frac{g_{k+1} - 2g_k + g_{k-1}}{\delta x^2} + \frac{3}{11}\frac{g_{k+2} - 2g_k + g_{k-2}}{4\delta x^2} \tag{4.2}$$

The fourth-order Runge-Kutta scheme for a random function z described as $z' = g(t, z)$, used in this research for time derivates of h and ρ in the model equations 3.1-3.4, is as follows:

$$k_1 = dt\ g(t_m, z_m) \tag{4.3}$$

$$k_2 = dt\ g(t_m + \frac{1}{2}dt, z_m + \frac{1}{2}k_1) \tag{4.4}$$

$$k_3 = dt\ g(t_m + \frac{1}{2}dt, z_m + \frac{1}{2}k_2) \tag{4.5}$$

$$k_4 = dt\ g(t_m + dt, z_n + k_3) \tag{4.6}$$

$$z_{m+1} = y_m + \frac{1}{6}(k_1 + 2k_2 + 2k_3 + k_4) \tag{4.7}$$

where k_1, k_2, k_3, k_4 are the four terms used for estimating $z(t_{m+1})$. $t_{m+1} = t_m + dt$ and z_{m+1} is the fourth-order Runge-Kutta calculation of $z(t_{m+1})$.

A comparison of sand surface, at $t = 32$ minutes, using a fourth order difference scheme for spatial derivates and a forward difference scheme for time derivatives with the ones used in this research is shown in Fig. 4.1. As can be seen from Fig. 4.1, ripple profile obtained by the fourth-order difference scheme has sharp edges and also is not successful in producing ripple shape asymmetry. On the other hand, the sixth-order difference scheme ripple profile is a lot smoother and realistic and hence this scheme is incorporated. For the purpose of comparison, the fourth-order difference scheme used is described by the equations 4.8 and 4.9.

The first derivative of a function g, at a point $x = k$, using a fourth-order difference scheme:

$$g_i' = -g_{k+2} + 8.0 \times g_{k+1} - 8.0 \times g_{k-1} + g_{k-2} \tag{4.8}$$

The second derivative of a function g, at a point $x = k$, using a fourth-order difference scheme:

$$g_i'' = -g_{k+2} + 16 \times g_{k+1} - 30.0 \times g_k + 16.0 \times g_{k-1} - g_{k-2} \tag{4.9}$$

The non-dimensional values of the constants, used for simulation runs, are shown in Table 4.1.

A rough sand surface has been used as the initial condition. The initial condition used for height of sand surface h is $h = 1.0 + 0.01r$ and for density ρ is $\rho = 2.6 + 0.01r$, where r is a random function used in fortran to generate random values between 0 and 1.

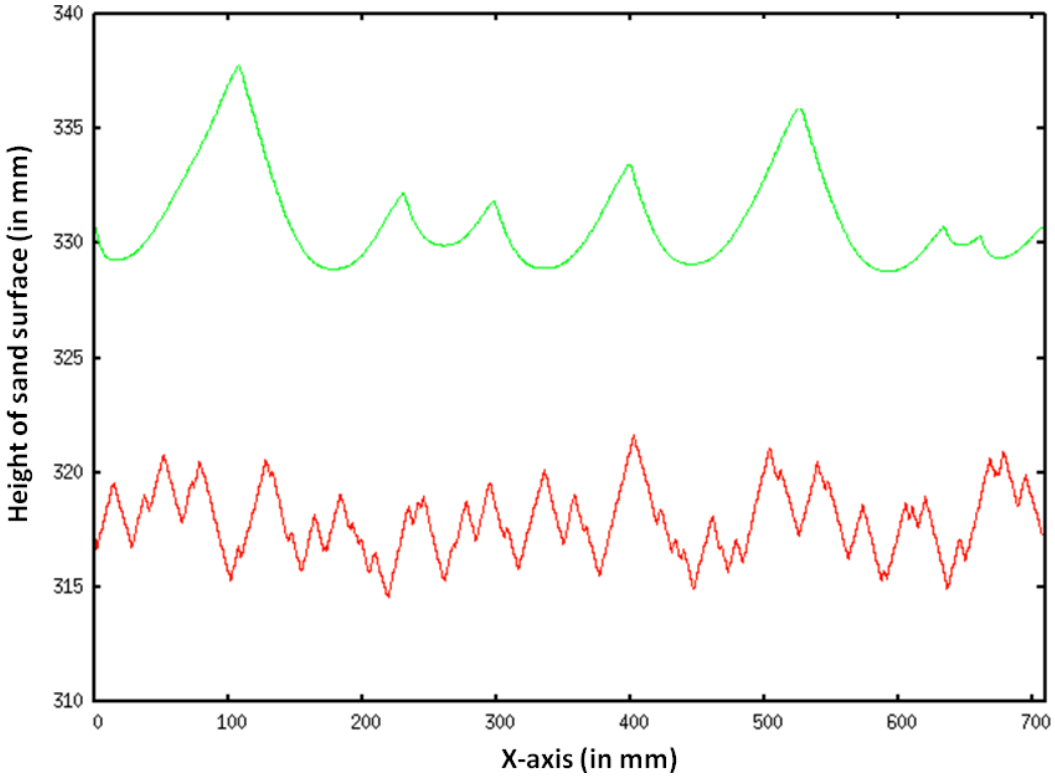

Fig. 4.1.: A comparison between the ripple surfaces at time $t = 32$ minutes obtained by using sixth-order difference scheme for spatial derivates, fourth-order Runge-Kutta scheme for time derivates (green) and by using fourth-order difference scheme for spatial derivatives, forward difference scheme for time derivatives (red)

Table 4.1: Values of numerical model constants

Constant	Values
$\frac{D_\rho}{D_h}$	1.0
$\frac{h_0}{\rho_0}$	20.0
$\hat{\chi}$	0.1
$\hat{\mu}$	1.0
$\hat{\kappa}$	0.1
β	25°
α	30°
γ	35°

The non-dimensional x co-ordinates are defined by dividing the total domain space of length $L = 50.0$ (non-dimensional space) into equal discrete intervals of $dx = 0.05$. Similarly, the total non-dimensional time domain $T = 0.3$ is divided into equal discrete intervals of $dt = 0.001$. The boundary conditions used are periodic in space with $h(nx) = h(nx-1) = h(nx-2)$ and $h(1) = h(2) = h(nx)$ at any time, where nx is the endpoint of the domain space for the space variable.

A normal distribution has been used for the probability function $p(a)$ with mean = 3.1 and variance = 0.1 (Hoyle and Mehta, 1999). In the equations 3.1- 3.4, tildes from $\tilde{t}$, $\tilde{x}$, $\tilde{h}$, $\tilde{\rho}$ have been ignored and hence t, x, h, ρ in the equations 3.1- 3.4 actually represent $\tilde{t}$, $\tilde{x}$, $\tilde{h}$, $\tilde{\rho}$. The non-dimensional values $\tilde{t}$, $\tilde{x}$, $\tilde{h}$, $\tilde{\rho}$, used and obtained from simulation runs, are then converted back to real physical values of time t, x-axis x, height of the surface h, and density of grains ρ using average radius of sand grains as 0.12 μm (same size as the ones used by the wind-tunnel experiments by Andreotti et al. (2006)). D_h, J, λ are calculated and substituted in the equations for t_0, x_0, h_0, ρ_0 as stated in the table 3.1. The resulting values are $t_0 = 160$, $x_0 = 14.2$ and $h_0 = 200$. The real physical values of t, x, h, ρ are then obtained by using $t = t_0\tilde{t}$, $x = x_0\tilde{x}$, $h = h_0\tilde{h}$, $\rho = \rho_0\tilde{\rho}$. Hence, t =160$\tilde{t}$, x =14.2 $\tilde{x}$ and h =200 $\tilde{h}$. Hence, the real domain chosen is 710 mm for x-axis and 48 minutes for time.

The code, in FORTRAN, is run and the simulation results are described below.

4.2 Ripple evolution results

Evolution of ripples beginning from a randomly disturbed bed of sand into a steady state of ripples is shown in Fig. 4.2. Fig. 4.2 also shows merging of ripple crests, by lines, to form bigger and stable ripples. Fig. 4.3 shows a comparison between the randomly disturbed sand bed at $t = 0$ and a steady-state ripple surface at $t = 32$ minutes. Fig. 4.4(a) and 4.4(b) show ripple evolution during the initial half of the evolution period and during later half over the whole length of the x-axis domain.

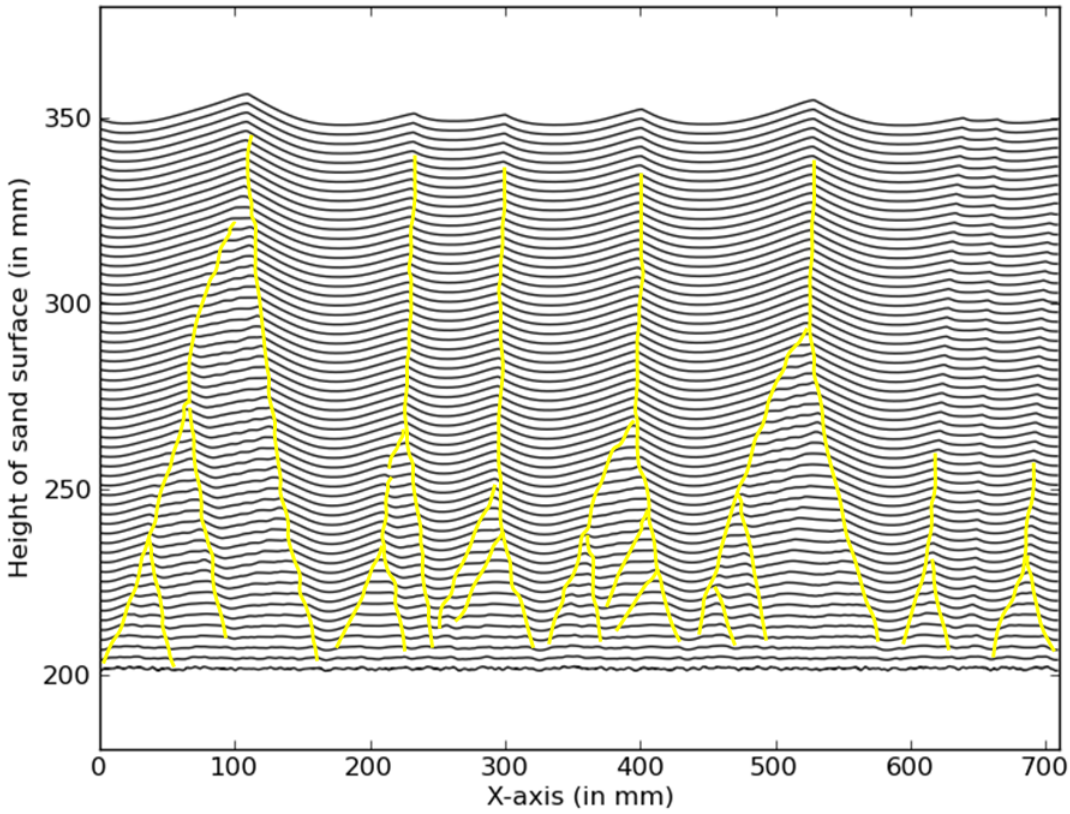

Fig. 4.2.: Spatio-temporal diagram of ripple evolution from $t = 0$ to $t = 37$ minutes with a time increment of 29 seconds. Yellow line joins a ripple's crestal point at different times.

It can also be seen from Fig. 4.4(b) that the irregular extrusions or small ditches on the bigger ripples get removed or get filled with time resulting in a smoother ripple profile. These figures show that, as time progresses, small ripples are formed on the disturbed sand surface and that these ripples coalesce to form steady-state big ripples. A good example of merging of two smaller ripples to form a single large ripple is shown in Fig. 4.9. Fig. 4.9(b) shows more snapshots of the merging ripples at intermediate times and a plot of crest-crest distance divided by crest-trough distance, at these times, is shown in Fig. 4.7. Fig. 4.7 shows that the ratio of crest-crest distance and crest-trough distance increases steeply with time and Fig. 4.9(b) shows how the original size of ripples changes as they merge with time. This observation reinforces

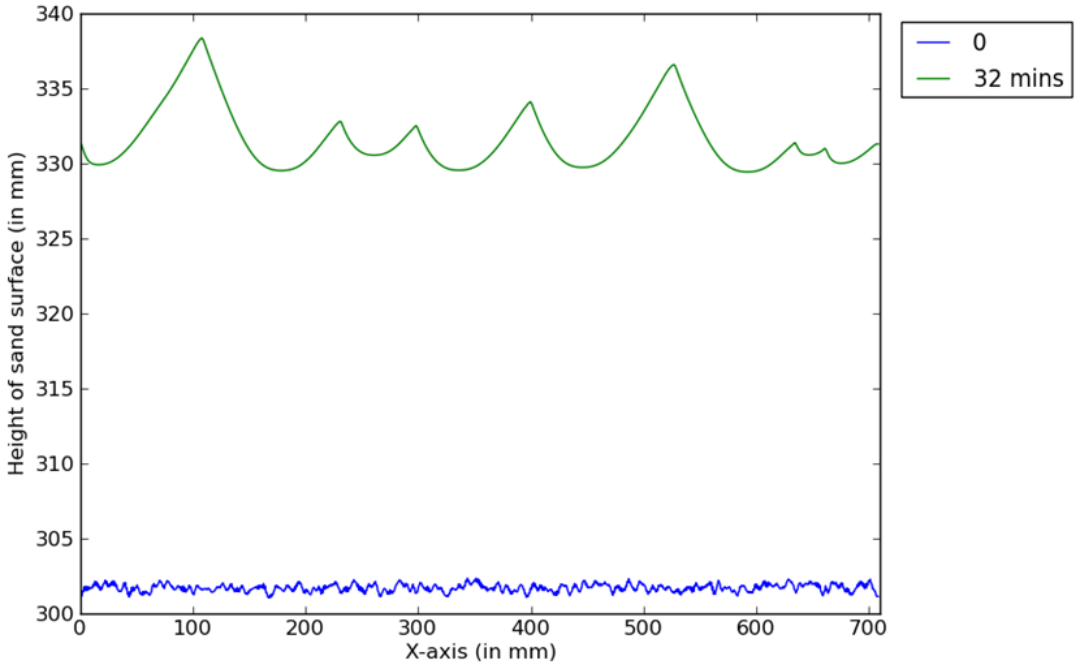

Fig. 4.3.: Comparison of ripple surface profiles at time $t = 0$ and $t = 32$ minutes. Sand surface at $t = 0$ is moved vertically up by 100 mm.

Forrest and Haff (1992)'s theory that as ripples merge, they interchange their size and essentially their velocity.

After a point of time, it is observed that ripples no longer evolve with the amplitude and wavelength remaining almost constant after this time. This time is referred to as the steady-state or equilibrium state. It can be seen from Fig. 4.8 that the steady-state is attained at about $t = 32$ minutes. The steady-state ripples, from Fig. 4.8, have an amplitude range of about 3 mm to 8.8 mm and a wavelength range of 8 cm to 16.4 cm. This wavelength and amplitude range is in reasonable agreement with the steady state amplitude range of about 5 to 10 mm and within the wavelength range of about 7 to 20 cm from the wind-tunnel experiments of Andreotti et al. (2006). As discussed earlier, it is observed that ripples do not evolve beyond $t = 32$ minutes and hence this time is chosen as the time taken to reach equilibrium state. This time is very much within the range of 22 minutes-36 minutes, actual

value being depending on the initial conditions, obtained from the wind-tunnel experiments of Andreotti et al. (2006). A detailed wavelength and amplitude study would aid in obtaining a stability diagram along the lines of Fig. 2.6.

A simulation run with a lower saltation angle $\beta = 20^\circ$ is tested and compared with saltation angle $\beta = 25^\circ$ as shown in Fig. 4.6(a). For lower saltation angles, the saltation lengths have not been changed and hence the initial wavelengths are similar but then the length of the shadow zone increases and hence the wavelength and height of the ripples are significantly different from those obtained originally as shown in Fig. 4.6(a). This observation is in accord with Sharp (1963)'s theory that the wavelength depends on the length of shadow zone. On the other hand, if the saltation angle is above the angle of repose then all the points on the sand surface are impacted by saltation and subsequently subjected to reptation. This prevents the formation of shadow zones and hence the growth of ripples and eventually the initially disturbed sand surface emerges as a flat sand surface as shown in Fig. 4.6(b).

With increase in time, the number of ripples appear to merge and the ripples tend to become more asymmetrical as they evolve towards steady state which is in accord with Anderson (1990). In Fig. 4.3, asymmetry of the steady-state ripples can be confirmed as the wind-ward side, of the first ripple from left, has an average slope of about 0.09 and the lee-ward side has an average slope of about 0.13. A similar trend in asymmetry is observed for other ripples in stead-state. Ripple index of the above mentioned ripple is about 16.54 which very much lies in the range of 15 to 20 as detected in the field by Cornish (1914). The distance between a local maximum to the very next local maximum is considered to be one ripple for simulation runs. Although, this is not a true definition of a ripple, this is chosen as a criteria for a simplified quantification of the ripples over its course of evolution. Fig. 4.5 shows how the number of ripples change with time.

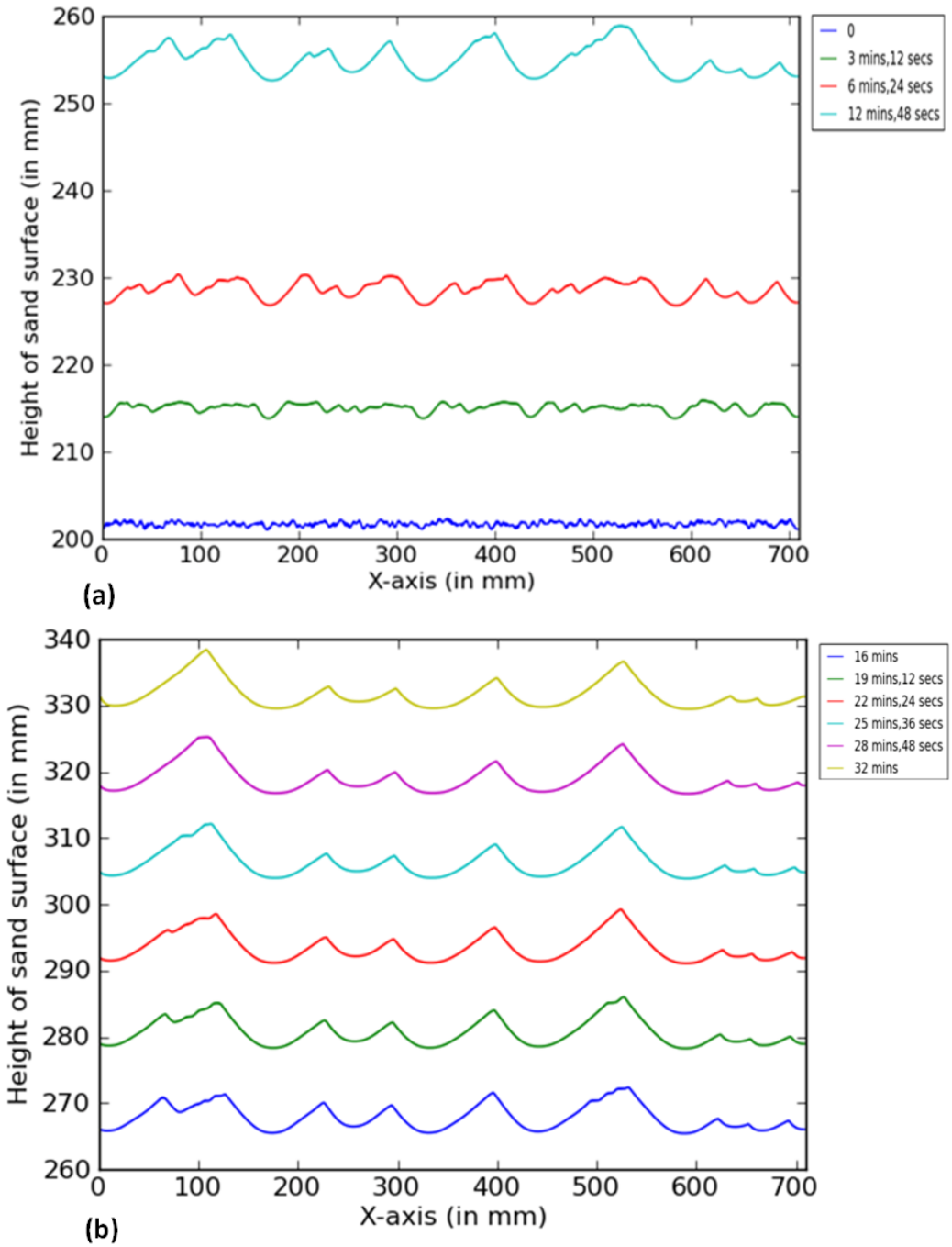

Fig. 4.4.: (a) Comparison between ripple surface profiles at initial times. (b) Comparison between ripple surface profiles at later times. Legend shows time.

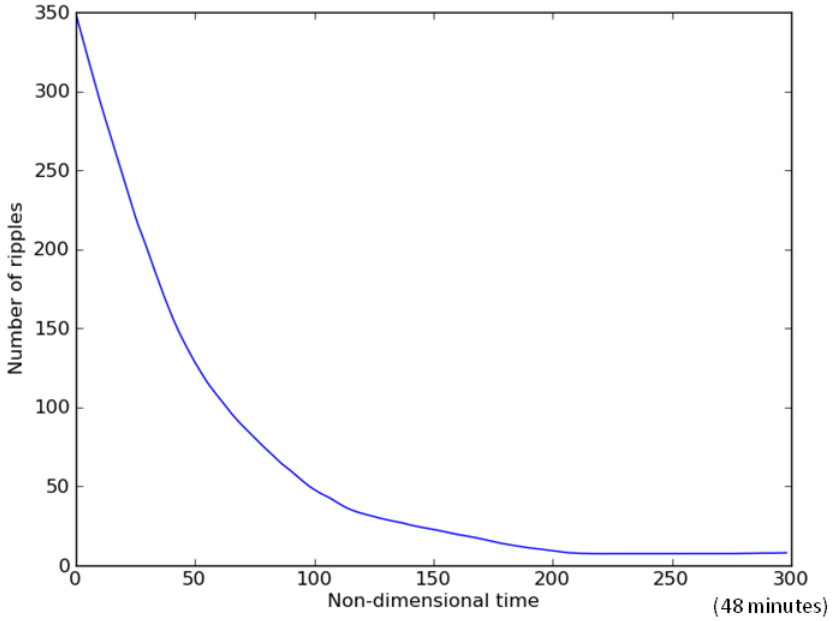

Fig. 4.5.: Number of ripples versus non-dimensional time. A moving average smoothing has been applied to the original data. Non-dimensional time $\tilde{t}$=300 stands for 48 minutes

The number of ripples decrease with time is because faster moving small ripples merge with other such ripples to form big ripples. Also, the rate at which the number of ripples decrease is much higher at beginning than at later times as shown in Fig. 4.5. As time reaches $t = 32$ minutes, the number of ripples almost do not decrease any more with time. This can be attributed to the steady state of ripples beyond which the ripples do not evolve in shape and size.

4.3 Contribution of terms

In the equations 3.1 and 3.3, each term represents a physical process responsible for the evolution of ripples from random bed surfaces. As discussed in the section "Analytical Description", $-\kappa\rho h_{xx}$ simulates the removal of excessive extrusions on the ripple crests and filling of ditches in the trough region of a ripple. This process is represented by the first term (term 1), $(1+\kappa\rho)\hat{h}_{xx}$, of the equations 3.1 and 3.3. For

ripple surface slopes less than $\tan\alpha$, the rolling grains would tend to adhere to the surface of the ripple and flow very slowly which is represented by the term $\lambda\rho(|h_x| - \tan\alpha)$. This process is modeled by the second term (term 2), $\rho\frac{\tan\beta}{\tan\alpha}(|h_x| - \frac{\tan\alpha}{\tan\gamma})$, of the equation 3.1. But at surface slopes greater than that of the angle of repose $\tan\alpha$, surface of a ripple is not stable as the grains are prone to avalanching which is modeled by the term $\upsilon(|h_x| - \tan\alpha)(\tan^2\gamma - h_x^2)^{-1/2}$. This process is modeled by the second term, $\frac{\hat{\upsilon}(|h_x| - \frac{\tan\alpha}{\tan\gamma})}{(1-h_x^2)^{1/2}}$, of the equation 3.3. Both the aforementioned process model rolling of grains under different scenarios but the contribution of hopping of grains alone in ripple evolution is modeled by the third term (term 3), $f(x) = (h_x + \frac{\tan\beta}{\tan\gamma})[1 + {h_x}^2\tan\gamma^2]^{-1/2}$, in both the equations 3.1 and 3.3. The contribution of these terms with time is discussed in this section. As per equations 3.1 and 3.3,

If $0 \leq h_x \leq \frac{\tan\alpha}{\tan\gamma}$, then

$$\begin{aligned} h_t &= (1 + \hat{\kappa}\rho)h_{xx} - \rho\frac{\tan\beta}{\tan\alpha}(|h_x| - \frac{\tan\alpha}{\tan\gamma}) - f(x) \\ &= (\text{term 1}) + (\text{term 2}) + (\text{term 3}) \end{aligned} \tag{4.10}$$

$$\frac{dh}{dt} = (\text{term 1}) + (\text{term 2}) + (\text{term 3}) \tag{4.11}$$

$$\begin{aligned} \text{dh} &= \text{dt} \times \text{term 1} + \text{dt} \times \text{term 2} + \text{dt} \times \text{term 3} \\ &= (\text{Term 1}) + (\text{Term 2}) + (\text{Term 3}) \end{aligned} \tag{4.12}$$

and similar terms Term 1, Term 2, Term 3 are also defined for the h_t equation 3.3 if $\frac{\tan\alpha}{\tan\gamma} \leq h_x \leq 1$. Term 1, Term 2, Term 3 are plotted at different times in the Fig. 4.10- 4.12. At an initial time $t = 3$ minutes and 12 seconds, it appears as if all the terms contribute more or less the same over the whole x-domain as shown in Fig. 4.10. However, at a later time $t = 16$ minutes, it appears as if Term 2, Term

3 are more or less similar in magnitude over the x-domain but Term 1 is lesser in magnitude around 1/3 to 1/2 of Term 2 or Term 3 as shown in Fig. 4.11. Another interesting observation made from Fig. 4.11 is that undulations in all the terms Term 1, Term 2, Term 3 begin to get localized and have major magnitude at the precise location of the ripples. At the bigger ripple on left and one on the right, in Fig. 4.11, the disturbances in Term 1, Term 2, Term 3 are still considerably consistent. This probably shows that this ripple is still undergoing reworking by the different processes and the other smaller ripples on the right are relatively more evolved. This inference is confirmed by looking at Fig. 4.12, occurring at $t = 32$ minutes, wherein all the terms Term 1, Term 2, Term 3 do not have much of a magnitude along the x-domain except at the ripple crest. As shown in Fig. 4.11- 4.12, Term 1 is lesser in magnitude than the Term 2 or Term 3 which can be attributed to a physical reasoning that at later times rolling does not play a major role in evolution of ripples. This confirms the generation of a steady state of ripples after which ripples do not evolve in shape and size.

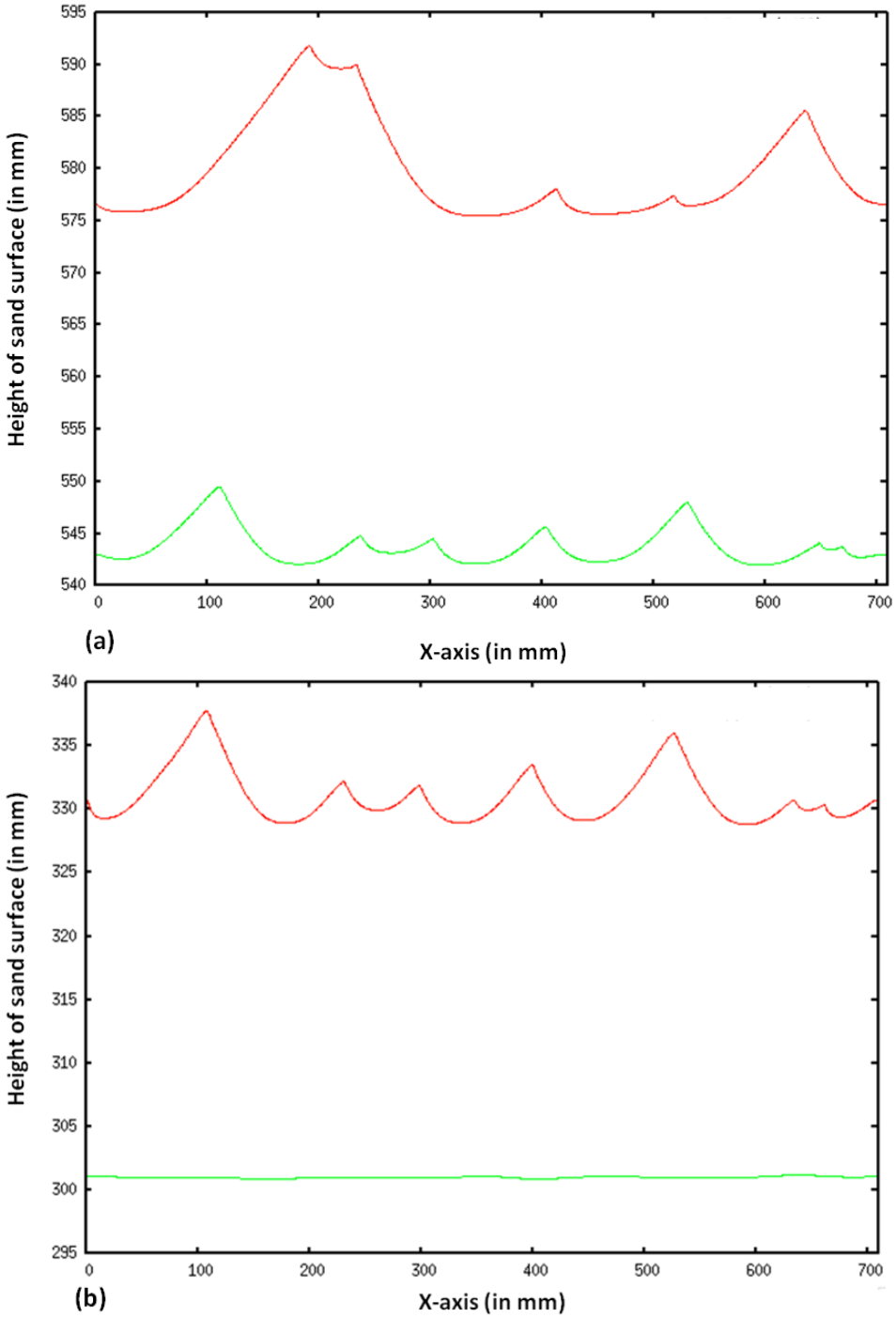

Fig. 4.6.: (a) A comparison between the ripple surfaces, obtained by $\beta = 20°$ (green) and $\beta = 25°$ (red), at time $t = 32$ minutes. (b) A comparison between the ripple surfaces, obtained by $\beta = 35°$ (green) and $\beta = 25°$ (red), at time $t = 32$ minutes.

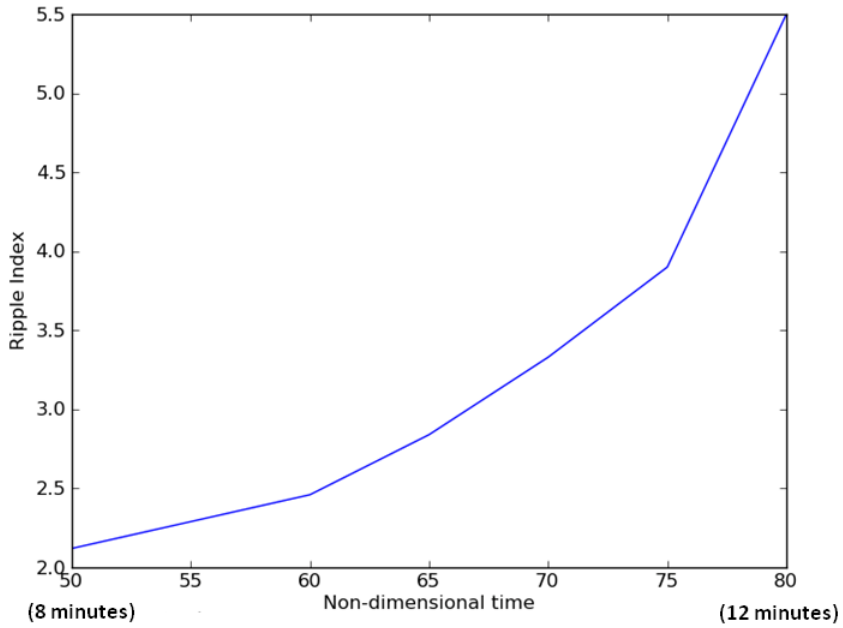

Fig. 4.7.: Crest-crest distance of the ripples divided by crest-trough distance against Non-dimensional time ($\tilde{t}$). $\tilde{t}$=50 stands for 8 minutes and $\tilde{t}$=80 stands for 12 minutes

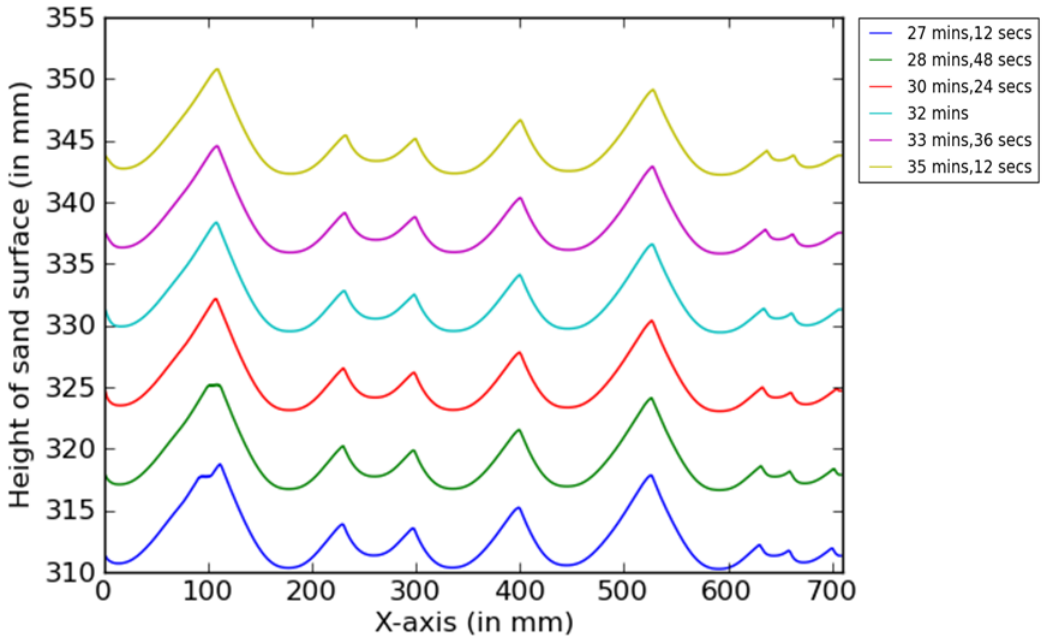

Fig. 4.8.: Comparison of ripple surface profiles at time t = 27 minutes and 12 seconds, t = 28 minutes and 48 seconds, t = 30 minutes and 24 seconds, t = 32 minutes, t = 33 minutes and 36 seconds, t = 35 minutes and 12 seconds

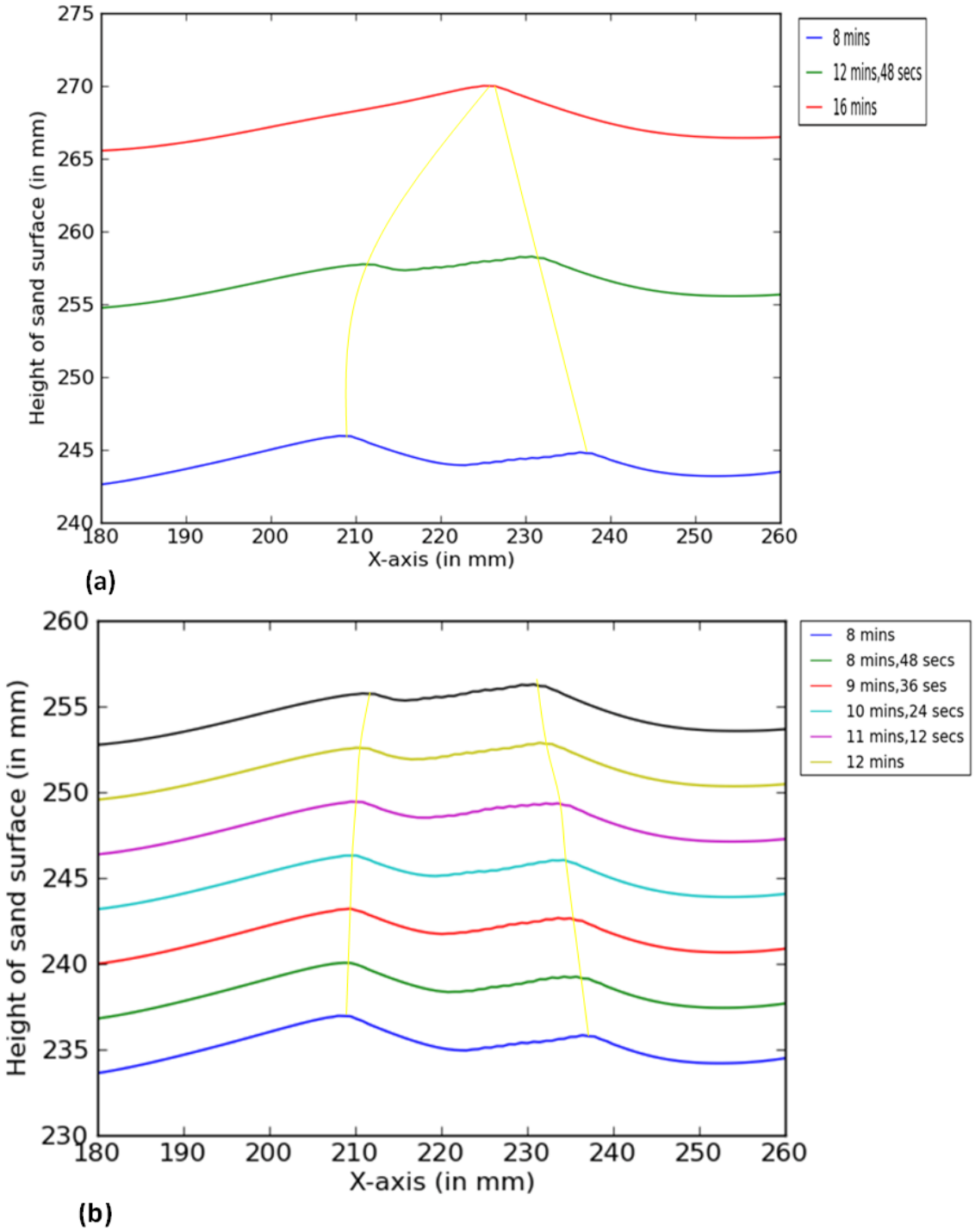

Fig. 4.9.: (a) Ripple surface profiles between $x = 180$ mm and $x = 260$ mm. Yellow lines join the crests of ripples at different times (b) Ripple surface profiles between the same x co-ordinates but various intermediate times. Yellow lines show merging of ripples and legend shows time.

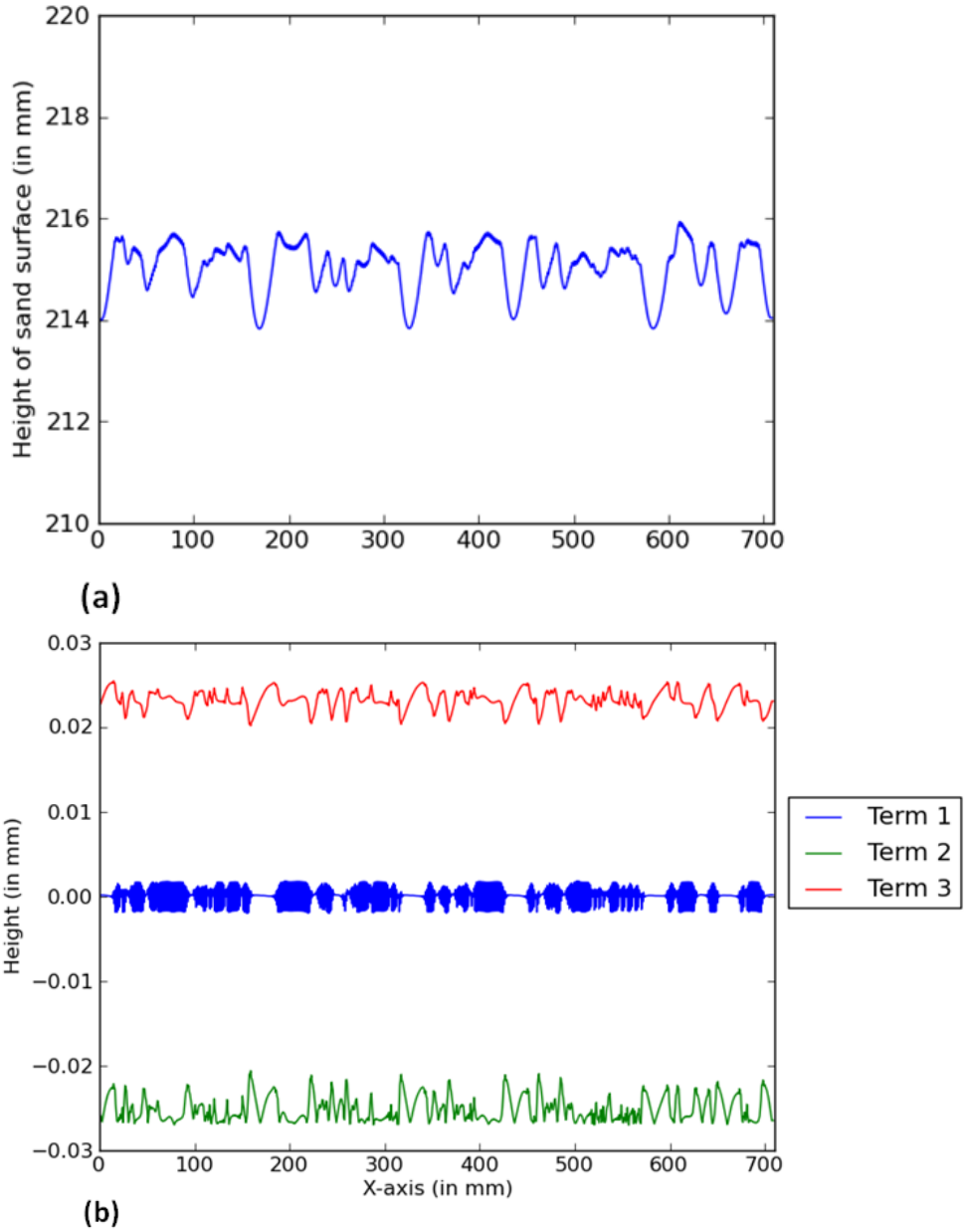

Fig. 4.10.: (a) Ripple surface profile at $t = 3$ minutes and 12 seconds (b) Contribution of Term 1, Term 2 and Term 3 at the same time $t = 3$ minutes and 12 seconds over the whole x-domain. Term 2 is moved up by 0.32 mm and Term 3 is moved down by 0.11 mm

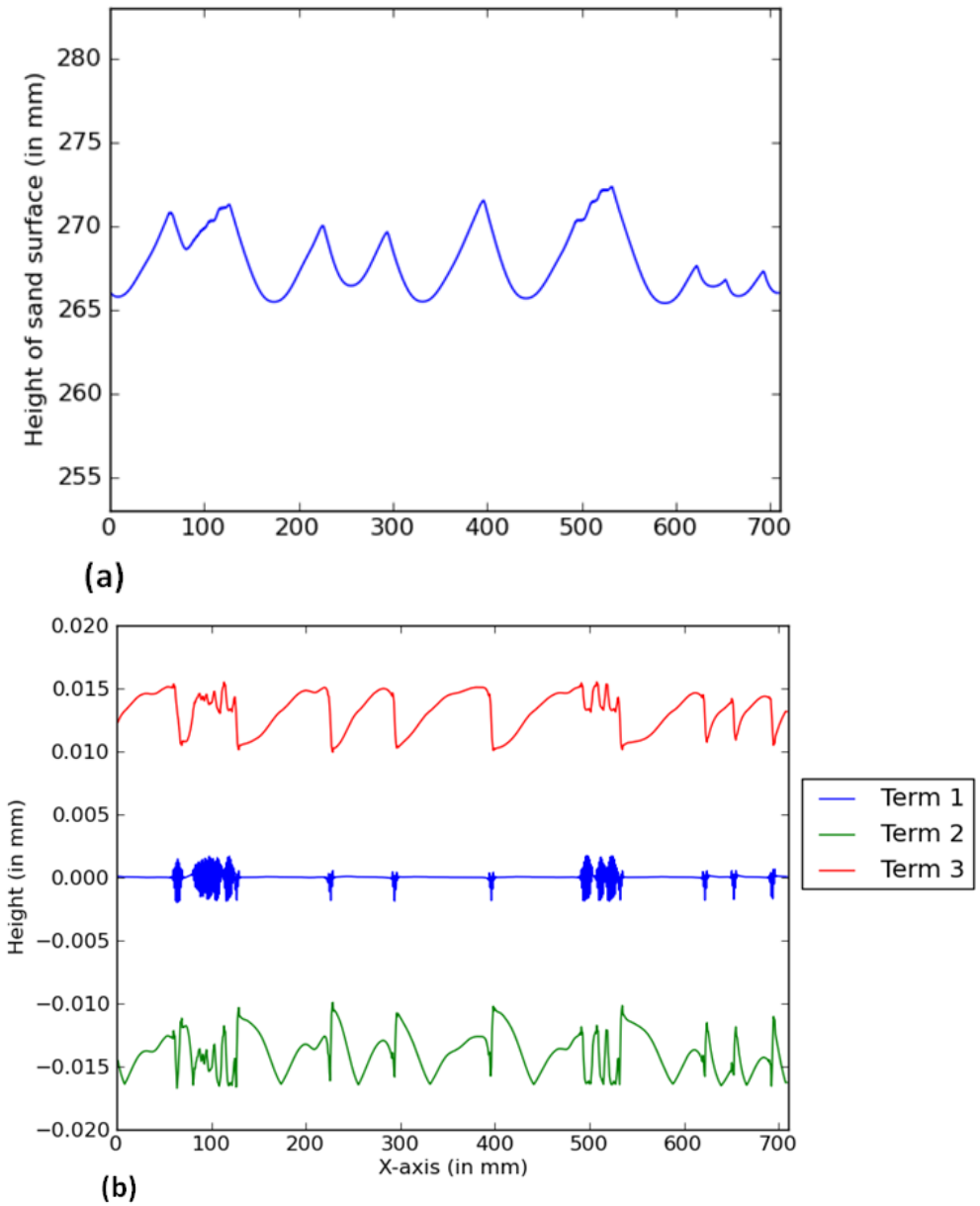

Fig. 4.11.: (a) Ripple surface profile at $t = 16$ minutes (b) Contribution of Term 1, Term 2 and Term 3 at the same time $t = 16$ minutes over the whole x-domain. Term 2 is moved up by 0.33 mm and Term 3 is moved down by 0.12 mm

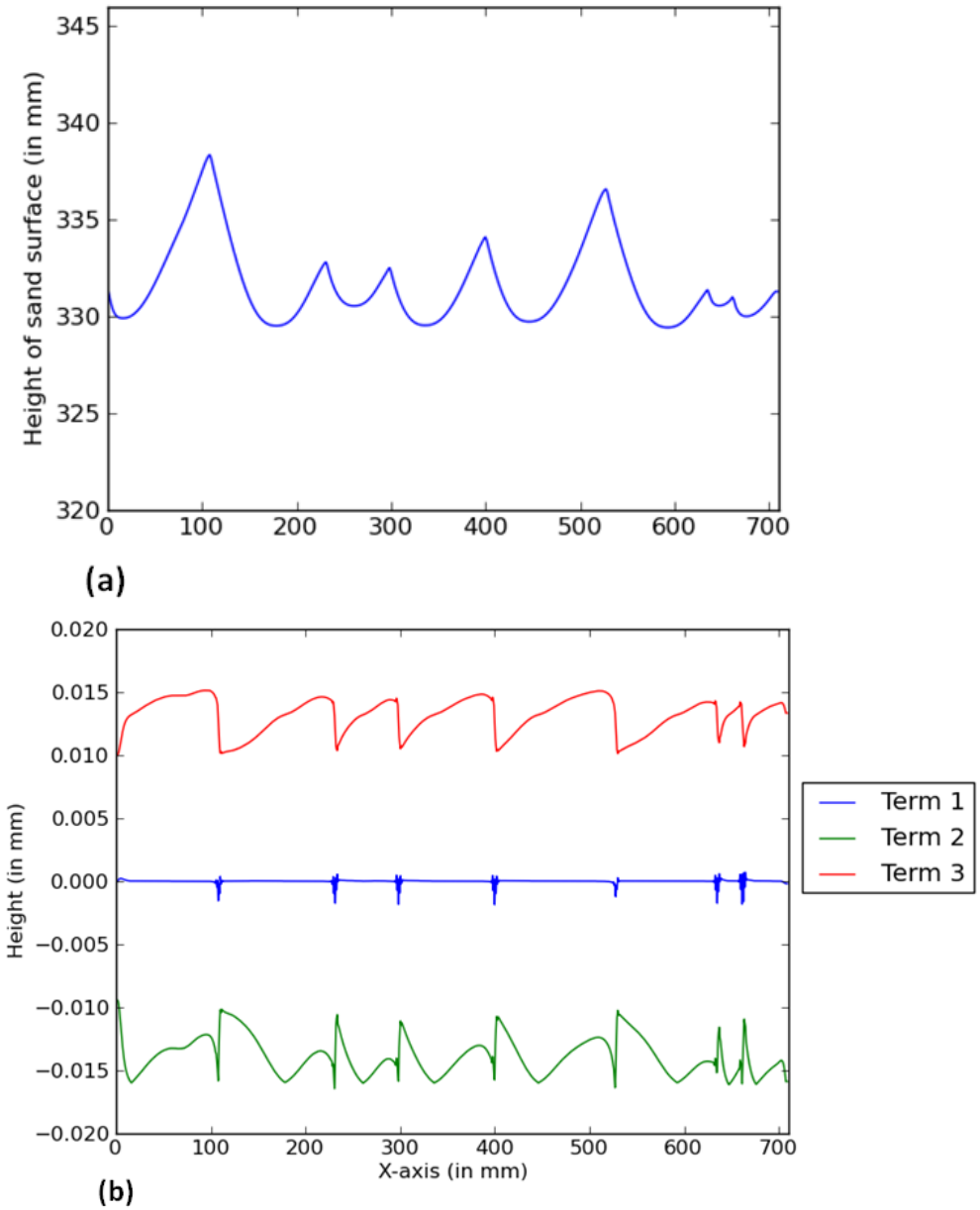

Fig. 4.12.: (a) Ripple surface profile at $t = 32$ minutes (b) Contribution of Term 1, Term 2 and Term 3 at the same time $t = 32$ minutes and over the whole x-domain. Term 2 is moved up by 0.33 mm and Term 3 is moved down by 0.12 mm

5. DISCUSSION

Wavelength and amplitude of the aeolian ripples consisting of a single grain size or of a unimodal grain size distribution usually ranges between 10-15 cm (Yizhaq et al., 2008) and less than 10 mm respectively. Amplitude range of the ripples obtained from the numerical model is 3 mm to 8 mm which is well within 10 mm. However, the numerical model assumes a single grain size. Sedimentary deposition record of migrating aeolian ripples with different grain sizes (within a unimodal distribution) have been observed to be inversely graded unlike subaqueous ripples. From the simulations, a hypothesis is that such sorting of grains with coarse grains on the crest acts as a shield against impinging fine grains would affect the ripples to grow bigger than subaqueous ripples producing higher ripple index values. Sand surfaces with a bimodal sand size distribution, with distinct coarse and fine size components, evolve into bed-forms which have much higher wavelength and amplitudes commonly referred to as "mega-ripples" (Tsoar, 1990). Mega-ripples have been found to have wavelengths ranging from about 25 cm to as high as 18 m (observed by (Milana, 2005) in Argentina) and amplitudes ranging from from a few centimeters to 1.8 m. Since the physical processes of transport remain the same for multiple grain sizes, it is postulated that Hoyle and Mehta (1999)'s model can be extended for "mega-ripples" with bimodal grain size distributions. Aeolian ripples which we observe commonly in sand are of unimodal distribution and consist predominantly of fine grains (Yizhaq, 2008). The reason is that, since the grains are more or less fine, the wind energy is sufficient to cause saltation of all the grains and hence the sorting of grains along the surface is not preserved. However, in case of "mega-ripples", wind-tunnel experiments by Walker (1981) have shown that coarse grains are less probable to be brought into saltation by wind and by impacting fine grains in saltation. This has been confirmed by field experiments conducted, by Jerolmack et al. (2006) along a dune filed at White Sands, New Mexico, USA and the authors came

to the conclusion that the threshold value of shear velocity for coarse grains would be the upper threshold value on wind speeds needed to produce grain sorting and growth of ripples. Jerolmack et al. (2006) also observed that reptation flux was much less in magnitude than saltation flux. In addition to sorting along crests and troughs, Tsoar (1990) observed, along aeolian ripples on a dune in the desert of Sinai, that the body of mega-ripples is composed mainly of fine grains with a layer or two of primarily coarse grains on the windward slope. This sorting and the formation of a layer of coarse grains on the wind-ward side, using Hoyle and Mehta (1999)'s model can be reproduced by making the flux of reptating grains dependent on the grain size. This can be achieved by using varying κ, λ constant values and varying ρ distributions according to grain size in equations 3.15 and 3.16. However, further line of inquiry is needed towards understanding how to change saltation flux. Enormous mega-ripples, which take years to form, can be studied only by means of numerical modeling and hence an extension of existing model to accommodate multiple grain sizes would help better understand the complex physical processes involved.

6. CONCLUSIONS

Numerical analysis of aeolian sediment transport helps in understanding the skill of a numerical model's in reproducing the bed-form geometries as obtained from laboratory based experiments like wind-tunnel experiments and field based observations. Thus, calibration of ripple evolution profiles help validate analytical models and analyze the effectiveness of an analytical model in simulating the different processes involved in development and evolution of ripples from random sand bed surfaces. This research is an attempt to address the aforementioned problem by conducting an elaborate validation of numerically obtained evolution results and understand the amends needed in the empirical equations to account for multiple sand grain sizes. The geometries of ripples produced, beginning from a random sand bed, from the simulation runs are compared with that of a particular wind-tunnel experiment.

To look back at the objectives, it was one of the goals to visualize equilibrium bed-forms and the time it takes to generate these conditions. The numerical model was successful in developing equilibrium bed-form state under steady-state conditions after about 32 minutes. Thus, the numerically modeled steady-state time lies very much within the equilibrium time period range of 22 to 36 minutes obtained from the wind-tunnel experiment, and hence proves the effectiveness in simulating equilibrium conditions. The second objective was to comprehend how well the ripple geometries reproduce those obtained by the wind-tunnel experiment. The wavelength of the equilibrium state ripples, produced from the numerical model, is the range of 3 mm to 8.8 mm which is in reasonable agreement with the range of 5 mm to 10 mm obtained from the wind-tunnel experiment. Wavelength, obtained from the numerical model, is in the range of 8 cm to 16.4 cm which is also in reasonable agreement with the range of 7 cm to 20 cm obtained from the wind-tunnel experiment. The numerical model was also successful in mimicking the asymmetrical shape of ripples.

Finally, the contribution of individual processes in shaping up the ripples with time is studied. The three processes, involved in the evolution of the height of ripples, are smoothing of ripple crests and troughs by rolling of grains, grains adhering to the surface at lower slopes and the contribution of hopping grains. It appears as if the three processes contribute more or less the same at initial times. However at later times, the process involved with the rolling of grains has lesser contribution compared to that of the hopping of grains and that of the grains adhering to the surface. This is perhaps a valid observation because at the beginning stages when smaller ripples merge, rolling plays an important role in shaping up and smoothing the bigger ripples and at a later time at which ripples are fully developed, saltation of grains from the crest and subsequent stable deposition is responsible for the fixed shape of the equilibrium state ripples.

For multiple grain sizes, it is hypothesized that making κ, λ and ρ distribution dependent on grain size would be a good methodology for achieving varying reptation flux and hence grain segregation. However, for a holistic approach, an analysis on how the saltation paths change with grain size and how it can be included in the currently applied model needs to be conducted.

REFERENCES

Anderson, R. S., 1987, A theoretical model for aeolian impact ripples: Sedimentology, **34**, 943–956.

———, 1990, Eolian ripples as examples of self-organization in geomorphological systems: Earth-Science Reviews, **29**, 77–96.

Anderson, R. S., and K. L. Bunas, 1993, Grain size segregation and stratigraphy in aeolian ripples modelled with a cellular automaton: Nature, **365**, 740–742.

Anderson, R. S., and P. K. Haff, 1988, Simulation of eolian saltation: Science, **241**, 820–823.

Anderson, R. S., and B. Hallet, 1986, Sediment transport by wind: Toward a general model: Geological Society of America Bulletin, **83**, 523–535.

Andreotti, B., P. Claudin, and O. Pouliquen, 2006, Aeolian sand ripples: Experimental study of fully developed states: Physical Review Letters, **96**, 028001–1–028001–4.

Baas, A. C., 2007, Complex systems in aeolian geomorphology: Geomorphology, **91**, 311–331.

Bagnold, R. A., 1941, The physics of blown sand and desert dunes: The Geographical Journal, **98**, 109–110.

Bouchaud, J.-P., M. E. Cates, J. R. Prakash, and S. F. Edwards, 1994, A model for the dynamics of sandpile surfaces: Journal De Physique I, **46**, 1383–1410.

Cornish, V., 1914, Waves of sand and snow: Fischer-Unwin, 288.

Forrest, S. B., and P. K. Haff, 1992, Mechanics of wind ripple stratigraphy: Science, **255**, 1240–1242.

Gamet, L., F. Ducros, F. Nicoud, and T. Poinsot, 1999, Compact finite difference schemes on non-uniform meshes. Application to direct numerical simulations of compressible flows: International Journal for Numerical Methods in Fluids, **29**, 159–191.

Hoyle, R. B., and A. Mehta, 1999, Two-species continuum model for aeolian sand ripples: Physical Review Letters, **83**, 5170–5173.

Hoyle, R. B., and A. W. Woods, 1997, Analytical model of propagating sand ripples: Physical Review E, **56**, 6861–6867.

Jensen, J. L., and M. Sorensen, 1986, Estimation of some eolian saltation transport parameters: A reanalysis of William's data: Sedimentology, **33**, 547–555.

Jerolmack, D. J., D. Mohrig, J. P. Grotzinger, D. Fike, and W. A. Watters, (2006), Spatial grain size sorting in eolian ripples and estimation of wind conditions on planetary surfaces: Application to Meridiani Planum, Mars: Journal of Geophysical Research-Planets, **111(E5)**.

Landry, W., and B. T. Werner, 1994, Computer simulations of self-organized wind ripple patterns: Physica D, **77**, 238–260.

Milana, J. P., 2005, Unique gravelly dunes at the windiest place of the world: a natural laboratory for wind-driven catastrophes: In: Holocene Environmental Catastrophes in South America: From the Lowlands to the Andes. Miramar, Argentina: Laguna Mar Chiquita.

Nishimori, H., and N. Ouchi, 1993, Formation of ripple patterns and dunes by wind-blown sand: Physical Review Letters, **71**, 197–200.

Pelletier, J. D., 2009, Controls on the height and spacing of eolian ripples and transverse dunes: A numerical modeling investigation: Geomorphology, **105**, 322–333.

Prigozhin, L., 1999, Nonlinear dynamics of aeolian sand ripples: Physical Review E, **60**, 729–733.

Sauermann, G., K. Kroy, and H. Herrmann, 2001, Continuum saltation model for sand dunes: Physical Review E, **64**, 031305.

Seppala, M., and K. Linde, 1978, Wind tunnel studies of ripple formation: Geografiska Annaler. Series A, Physical Geography, **60**, 29–42.

Sharp, R. P., 1963, The Wind Ripples: The Journal of Geology, **71**, 617–636.

Tsoar, H., 1990, Grain-size charateristics of wind ripples on a desert seif dune: Geography Research Forum, **10**, 37–50.

Walker, D. J., 1981, An experimental study of wind ripples: M.Sc. thesis, Massachusetts Institute of Technology.

Werner, B. T., 1995, Eolian dunes: Computer simulations and attractor intepretation: Geology, **23**, 1107–1110.

Werner, B. T., and D. T. Gillespie, 1993, Fundamentally discrete stochastic model for wind ripple dynamics: Physical Review Letters, **71**, 3230–3234.

Yizhaq, H., 2008, Aeolian megaripples: Mathematical model and numerical simulations: Journal of Coastal Research, **24**, 1369–1378.

Yizhaq, H., N. J. Balmforth, and A. Provenzale, 2004, Blown by wind: Nonlinear dynamics of aeolian sand ripples: Physica D, **195**, 207–228.

Yizhaq, H., O. Isenberg, R. Wenkrat, and H. Tsoar, 2008, Aeolian megaripples as a self-organization phenomenon: Mathematical modeling, field Studies and implications to martian megaripples: Planetary Dunes Workshop: A Record of Climate Change, **157**, 875–897.